EFFECTS OF BLOWING RATIOS ON HEAT TRANSFER TO THE THROAT REGION OF A POROUS-WALLED NOZZLE

THESIS

Fu-Jung Chen
Major,ROCAF

AFIT/GAE/ENY/95J-01

DEPARTMENT OF THE AIR FORCE
AIR UNIVERSITY
AIR FORCE INSTITUTE OF TECHNOLOGY

Wright-Patterson Air Force Base, Ohio

AFIT/GAE/ENY/95J-01

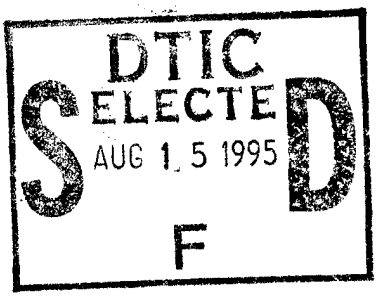

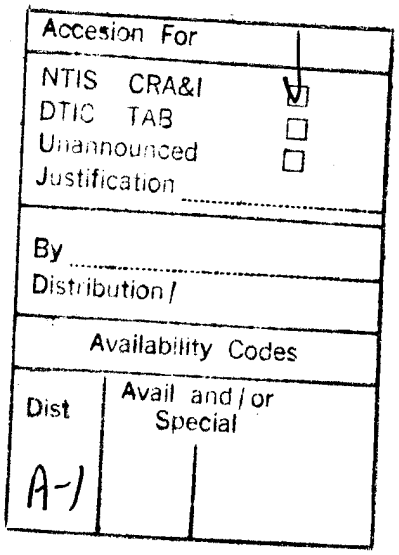

EFFECTS OF BLOWING RATIOS ON HEAT TRANSFER TO THE THROAT REGION OF A POROUS-WALLED NOZZLE

THESIS
Fu-Jung Chen
Major,ROCAF

AFIT/GAE/ENY/95J-01

AFIT/GAE/ENY/95J-01

EFFECTS OF BLOWING RATIOS ON HEAT TRANSFER TO THE THROAT REGION OF A POROUS-WALLED NOZZLE

THESIS

Presented to the Faculty of the Graduate School of Engineering
of the Air Force Institute of Technology
Air University
In Partial Fulfillment of the
Requirements for the Degree of
Master of Science in Aeronautical Engineering

Fu-Jung Chen, B.S.
Major,ROCAF

June, 1995

Preface

This study continues the transpiration cooling research done in the AFIT Low Pressure Shock Tube by previous researchers. The focus of this study, other than to observe the effects of transpiration cooling on the nozzle exit Mach number, was to understand the effectiveness of transpiration cooling on the nozzle throat. Although transpiration cooling is not a new idea to cool the nozzle, it still hasn't had any analytical or empirical solution. Hence, more experiments are required for further research.

This experiment would not have been possible without the help of several people. My greatest thanks go to my advisor, Lt Col. Jerry Bowman who always made himself available to answer my questions and correct my thesis with patience and good humor. My appreciation also goes to Dr. Rodney Bowersox who helped me to set up the Shadowgraph system and answered many questions, and Dr. Franke who helped me to correct my thesis. Without these people's help, completion of this thesis would have been impossible. My thanks also go to Mr. Jay Anderson, Lab supervisor, and Mr. Andrew Pitts for their help with all the hardware concerns surrounding this subject. Finally, I want to thank my wife Jane and three children for their understanding and patience.

Fu-Jung Chen

Table of Contents

List of Figures

List of Tables

List of Symbols

Symbol	Description	Units
a	Sound Speed	$\frac{m}{sec}$
A_i	Injection Surface Area	m^2
A_p	Nozzle Cross Sectional Area	m^2
BR	Blowing Ratio	
c	Specific Heat of a Solid	$\frac{J}{kgK}$
c^*	Characteristic Velocity	$\frac{m}{sec}$
c_p	Specific Heat at Constant Pressure	$\frac{J}{kgK}$
D_*	Nozzle Throat Diameter	m
h	Convective Heat Transfer Coefficient	$\frac{W}{m^2K}$
k	Thermal Conductivity	$\frac{W}{mK}$
$\dot{m}$	Mass Flow Rate	$\frac{kg}{sec}$
M	Mach Number	
M_P	Shock Wave Mach Number	
M_R	Reflected Shock Wave Mach Number	
p	Static Pressure	Pa
P	Total Pressure	Pa
p_{plenum}	Plenum Pressure	Pa
Pr	Prandtl Number $(\frac{c_p \mu}{k})$	
q''	Heat Flux	$\frac{W}{m^2}$
r	Recovery Factor	
r_c	Throat Radius of Curvature in Downstream Direction	m
t	Time	sec
T	Temperature	K
u	Velocity	$\frac{m}{sec}$

W	Shock Wave Speed	$\frac{m}{sec}$
W_R	Reflected Shock Wave Speed	$\frac{m}{sec}$
α	Thermal Diffusivity	$\frac{m^2}{sec}$
γ	Ratio of Specific Heats $(\frac{c_p}{c_v})$	
μ	Dynamic Fluid Viscosity	$\frac{Nsec}{m^2}$
ρ	Density	$\frac{kg}{m^3}$
σ	Stefan Boltzmann Constant	

Subscripts

0	Stagnation Condition
1	Condition in the front of Shock Wave
2	Condition Behind the Shock Wave
3	Condition After the Rarefaction Wave
4	Driver Section Condition
5	Condition Behind the Reflected Shock Wave
aw	Adiabatic Wall
g	Primary Gas
i	Injection Flow
p	Primary Nozzle Flow
w	Inner Wall Surface Condition
*	Nozzle Throat Condition

AFIT/GAE/ENY/95J-01

Abstract

The effects of transpiration cooling on heat transfer in the throat region of a porous-walled nozzle were investigated. The experiments were performed in the AFIT low speed shock tube fitted with a Mach 2 nozzle. A blowing region was limited to the area from 1.3 cm prior to the throat to 1.2 cm downstream of the throat. The blowing ratios from -0.0002 (suction) to 0.0117 (blowing) of the main stream flow were studied.

Heat flux data were taken from both sides of the nozzle. One side was transpiration cooled by secondary air injection through a porous wall, while the other side was an impermeable surface. The transpiration cooled side results showed up to a 40% reduction in heat transfer coefficient at the blowing ratio of 0.0116. Also, with this small blowing region (from 1.3 cm upstream of the nozzle throat to 1.2 cm downstream of the nozzle throat), the results of the exit Mach number and boundary layer thickness showed good improvement compared to a larger blowing region (from 1.3 cm upstream of the throat to 8.8 cm downstream of the throat).

EFFECTS OF BLOWING RATIOS ON HEAT TRANSFER TO THE THROAT REGION OF A POROUS-WALLED NOZZLE

I. INTRODUCTION

1.1 Background

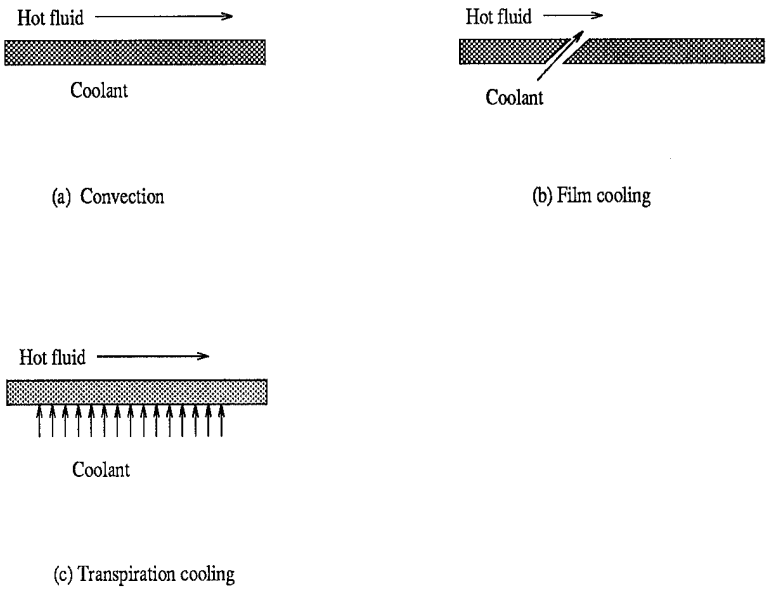

Figure 1.1 Schematic Representation of Convection, Film, and Transpiration Cooling

One way to increase the performance of turbine and rocket engines is to increase the combustion chamber temperature. This high temperature environment influences the endurance of the wall's material (especially in the nozzle throat). Special cooling methods have been developed to protect the surface from the influence of a hot gas stream. Fig 1.1 presents sketches of these cooling methods. Fig 1.1(a) shows conventional convection cooling in which the hot fluid is on one side and coolant is

on the other side. Fig 1.1(b) shows the film cooling process, in which a stream of coolant is blown through an opening at some angle to the surface. In this way a boundary layer is created by the secondary fluid to insulate the wall from the hot fluid. This film is gradually destroyed when the secondary fluid and hot fluid are mixed together. Therefore the downstream surface will no longer be protected by the film. This disadvantage can be avoided by using transpiration cooling. Fig 1.1(c) shows the transpiration process, in which a stream of coolant is injected normal to the boundary layer through a uniformly porous material. The coolant thus serves as a suitable heat sink within the walls of the structure and a protective film which decreases the effective convective heat coefficient along the surface.

In this research, the scope was restricted to transpiration cooling. Eckert and Livingood (5) compared film cooling and transpiration cooling with conventional convection and found that, on the basis of equal coolant flow rates, transpiration cooling was the most effective system.

1.2 Problem Statement

The heat transfer rates of rocket propulsion are usually very high in the combustion chamber and nozzle due to the high combustion chamber temperature. Typically, the combustion temperatures are usually two times the melting point of steel (14). A failure normally occurs when some part or component becomes too hot, so that it no longer functions properly. Each component has its limit temperature that should not be exceeded. These limits are usually established by available material.

Because the heat exchange relations through the turbulent layer near the wall of a supersonic nozzle are very complex, no generalized analytical solution exists for the prediction of heat flux in the nozzle. This leaves the empirical approach as the best method to predict heat flux. A heat transfer empirical relationship has been developed for predicting the heat transfer coefficient from hot gas flow to the wall of

the nozzle (3), but experimental research is necessary to correlate heat transfer with blowing ratio.

1.3 Summary of Current Knowledge

Experimental research in the area of transpiration cooling had been conducted since 1946. The first successful full scale demonstration of transpiration cooling occured in 1967 with the firing of the Aerojet ARES, a 100,000 pound (445 KN) thrust chamber (9). Transpiration cooling was also successfully used to cool injector faces in the upper stage engine (J-2) of the moon launch vehicle and space shuttle main engine (SSME) with hydrogen fuel (14).

Mickley et al (10) theoretically and experimentally studied the effect of blowing or sucking air through a porous flat plate into or out of a main air stream flowing parallel to the plate on the boundary layer. Theory and experiment showed qualitative agreement. Suction decreased the boundary layer thickness, increased the magnitude of the friction and heat transfer and delayed the transition from laminar to turbulent flow. Blowing increased the boundary layer thickness, decreased the magnitude of the friction and heat transfer, and hastened the transition from laminar to turbulent flow.

Transpiration cooling has not been successful in cooling combustion chamber or nozzle walls because the pressure drop across the inner thrust chamber wall varies along the axis of the chamber, particularly in the nozzle region (14). Librizzi and Cresci (8) presented the results of an experimental investigation of the downstream influence of mass transfer on heat transfer to an axisymmetric nozzle in turbulent flow. Helium and nitrogen, used as coolants, were injected through a porous region upstream of the nozzle throat at various rates. The results showed a decrease in heat transfer rate with an increase in mass injection. This decrease in heat transfer rate became less prominent as the distance downstream of the porous region increased. Lenertz (7) experimentally investigated transpiration cooling in the throat region of

a two-dimensional nozzle. The upper side of the nozzle studied was an impermeable surface while the bottom side was a porous material. Coolant was injected into the nozzle through the porous material. The result showed a 14% reduction in heat transfer rate using a blowing ratio of 0.0051 with virtually no loss in performance. Keener (6) showed a growth in the velocity boundary layer thickness due to mass injection through the nozzle wall. This lead to a reduction of local Mach number at the nozzle exit.

1.4 Scope and Objective

Because of the complex nozzle geometry, the scope of this research was limited to measure the effectiveness of transpiration cooling in the throat region of a supersonic nozzle at low blowing ratios. The AFIT low pressure shock tube was used. A high velocity flow behind a shock wave was created to simulate a steady state high temperature flow. The injected fluid was identical to the main stream. The nozzle used was the same as used by Lenertz, except the blowing section was shortened. Temperature data were acquired from both nonblowing and blowing sides of the nozzle at the location where the flow Mach number was M=1.17.

The main objective of this research was experimentally to understand the differences between flow over a porous wall with blowing and non porous wall with no blowing and to relate blowing ratio to heat transfer rate and coefficient. The effect of blowing ratio on boundary layer thickness was also studied.

1.5 Methodology

A Mach 2 nozzle was designed by method of characteristic and installed into the shock tube. The driver section of the shock tube was pressurized. A diaphragm was ruptured generating a shock wave. This shock wave propagated down the tube at the supersonic speed into the driven section which was at a pressure lower than that of the driver section. After the shock wave passed the nozzle located at the end

of the shock tube, the gas temperature suddenly increased causing heat energy to be transferred to the nozzle.

Since the run times in the shock tube were very short, fast response instruments were required in the test. Medtherm thin-film resistance gauges made of a platinum film deposited on a corning Pyrex 7740 substrate and Endevco model 8530A-100 piezoresistive pressure transducers were used to meet this requirement. A total of 11 pressure transducers were used to collect the data necessary for analysis. They were placed in the diverging section of the nozzle to measure the static pressure, in the converging section of the nozzle to measure the stagnation pressure, in the pitot tube for exit total pressure measurement, in the constant pressure blowing plenum and along the top of the shock tube for shock wave speed measurement. Two thin-film resistance gauges were placed in the throat region of the nozzle walls to measure the temperature at each wall.

The voltage output during a run was collected and stored by the Nicolet 500 Data Acquisitions system, and then were transformed into temperature output through a known physical characteristic of a particular heat flux gauge.

A dynamic calibration determined the thermal product ($\sqrt{\rho ck}$). Once the thermal product was known, the temperature profile during a run will yield the heat transfer rate as a function of time. This heat transfer rate was then averaged over the run time, and divided by a temperature difference to find the heat transfer coefficient:

$$h = \frac{q''}{T_{aw} - T_w} \tag{1.1}$$

where q'' is the heat transfer rate per unit area, h is the convective heat transfer coefficient, T_{aw} is the adibatic wall temperature and T_w is the actual wall temperature.

A blowing ratio was defined as

$$BR = \frac{\dot{m}_i / A_i}{\dot{m}_p / A_p} = \frac{\rho_i u_i}{\rho_p u_p} \tag{1.2}$$

where $\dot{m}_i$ and A_i are the mass flow rate and the area of injection and $\dot{m}_p$ and A_p are mass flow rate and area of primary flow. The symbols ρ and u represent density and velocity respectively. Since the pressure along the nozzle wall wasn't constant, the velocity exiting the porous wall was not constant along the wall. This made the blowing ratio more difficult to calculate. A program was written (7) to numerically integrate the mass injection along the wall to get a cumulative blowing mass flow rate upstream of the heat flux gauge. When the plenum pressure is lower than the pressure along the wall, the blowing ratio is negative. The blowing ratio would be positive only if the plenum pressure is larger than the nozzle wall pressure at some location or over all the porous material in front of the gauge. A relationship for blowing ratio vs. the ratio of heat transfer coefficient between blowing and nonblowing wall was then obtained.

II. THEORY

2.1 Shock Tube

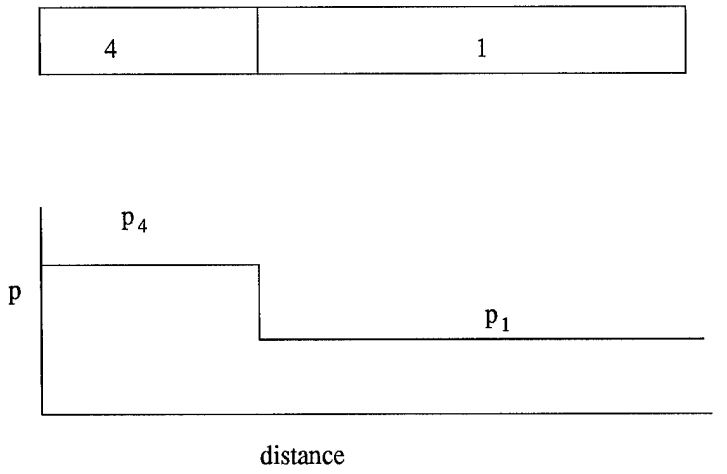

(a) initial condition in a pressure-driven shock tube

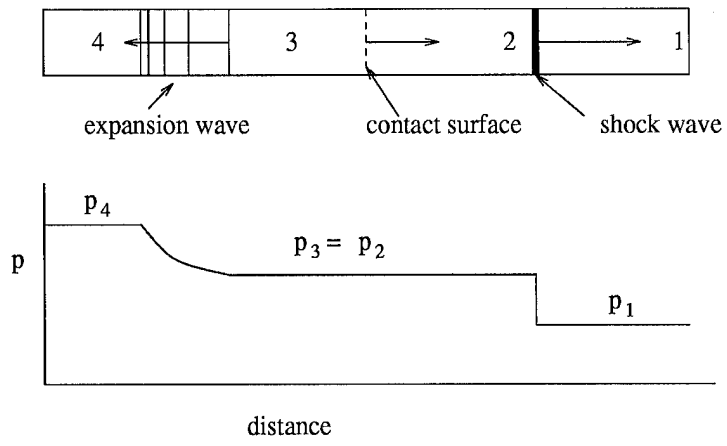

(b) flow in a shock tube after the diaphragm is broken

Figure 2.1 Schematic of Simple Shock Tube

Fig 2.1 shows the most simple shock-tube assembly. The shock tube consists of a rigid duct divided into two sections by a gas tight diaphragm. The left-hand side, known as a driver section, contains a gas at the pressure p_4 which is in excess of the pressure p_1 of the gas on the right-hand side of the tube known as a driven section. When the diaphragm is broken, a right-traveling shock propagates into the driven section and a left-traveling rarefaction travels into the driver section. Behind the shock wave is a flow of gas and in order to avoid pressure variations building up the flow velocity is uniform in the region between the tail of shock wave (denoted by region 2) and the tail of the rarefaction wave (denoted by region 3). This is also a region of constant pressure. That is $p_2 = p_3$ and $u_2 = u_3$ (17). However, since region 3 and 4 are isentropic and since there is an entropy increase across the shock from 1 to 2, the temperature in zones 2 and 3 are not alike. Therefore, a contact discontinuity of temperature separates these two regions (13).

The pressure, temperature and density ratio across the shock wave for a right-traveling shock is expressed (1)

$$\frac{p_2}{p_1} = 1 + \frac{2\gamma}{\gamma+1}[(\frac{W}{a_1})^2 - 1] \tag{2.1}$$

$$\frac{T_2}{T_1} = \frac{p_2}{p_1}(\frac{\frac{\gamma+1}{\gamma-1} + \frac{p_2}{p_1}}{1 + \frac{\gamma+1}{\gamma-1}\frac{p_2}{p_1}}) \tag{2.2}$$

$$\frac{\rho_2}{\rho_1} = \frac{1 + \frac{\gamma+1}{\gamma-1}\frac{p_2}{p_1}}{\frac{\gamma+1}{\gamma-1} + \frac{p_2}{p_1}} \tag{2.3}$$

where W is shock speed, a_1 is a sound speed at region 1. Given the measured shock speed and knowing the driven section pressue p_1 and temperature T_1, the test condition pressure p_2, temperature T_2 may be computed, and velocity in the region 2 can be computed by equation

$$u_2 = \frac{a_1}{\gamma}\left(\frac{p_2}{p_1} - 1\right)\sqrt{\frac{\frac{2\gamma}{\gamma+1}}{\frac{p_2}{p_1} + \frac{\gamma-1}{\gamma+1}}} \tag{2.4}$$

If the duct is a closed end duct, a reflected normal shock wave will reflect from the closed end and travel to the left with velocity W_R, and the flow speed behind the reflected shock wave is zero. Fig 2.2 shows the reflected shock wave and denotes a state 5 after the shock wave reflects from the wall.

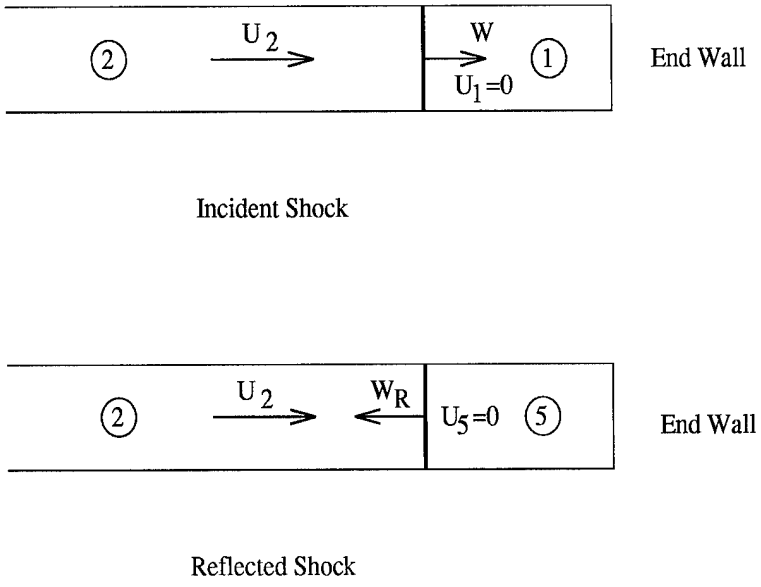

Figure 2.2 Incident and Reflected Shock Wave

The continuity, momentum, and energy equation for a reflected shock wave can be written as (1):

$$\rho_2(W_R + u_2) = \rho_5 W_R \tag{2.5}$$

$$p_2 + \rho_2(W_R + u_2)^2 = p_5 + \rho_5 W_R^2 \tag{2.6}$$

$$h_2 + \frac{(W_R + u_2)^2}{2} = h_5 + \frac{W_R^2}{2} \tag{2.7}$$

and a relation between propagated shock wave Mach number M_P and reflected shock wave Mach number M_R can be expressed as:

$$\frac{M_R}{M_R^2 - 1} = \frac{M_P}{M_P^2 - 1}\sqrt{1 + \frac{2(\gamma - 1)}{(\gamma + 1)^2}(M_P^2 - 1)[(\gamma + 1)\frac{1}{M_P^2}]} \tag{2.8}$$

and

$$M_R = \frac{(W_R + u_2)}{a_2} \tag{2.9}$$

Where W_R is the reflected wave speed. Once the shock wave speed W is known, the simulated combustion chamber pressure p_5, Temperature T_5, and density ρ_5 can be obtained from Eqs (2.5),(2.6),(2.7),(2.8) and (2.9).

2.2 Heat Transfer

Newton's law of cooling for heat transfer rate per unit area from a gas flow to a wall can be expressed as

$$q'' = h(T_{aw} - T_w) \tag{2.10}$$

For a high speed flow, a recovery factor r is defined as

$$r = Pr^{1/3} = \frac{T_{aw} - T_g}{T_0 - T_g} \tag{2.11}$$

where Pr is the Prandtl number. For air $Pr = 0.71$, $r = 0.89$ and T_0 is the stagnation temperature. Eq(2.11) can be rearranged as

$$T_{aw} = T_g(1 + r\frac{\gamma - 1}{2}M^2) \tag{2.12}$$

where γ is the specific heat ratio and M is the primary flow Mach number. Therefore Eq(2.10) becomes

$$h = \frac{q''}{T_g(1 + r\frac{\gamma-1}{2}M^2) - T_w} \tag{2.13}$$

An expression for convective heat transfer in a supersonic nozzle is given by Bartz (3) as follows:

$$h = [\frac{0.026}{(D_*)^{0.2}}(\frac{D_*}{r_c})^{0.1}(\frac{\mu^{0.2}c_p}{Pr^{0.6}})(\frac{P_0}{c^*})^{0.8}](\frac{A_*}{A})^{0.9}\sigma \tag{2.14}$$

where the asterisk subscript indicates condition at the nozzle throat, the zero subscript indicates stagnation conditions, r_c is the throat radius of curvature along the direction of flow, c^* is the rocket performance parameter characteristic velocity, P_0 is the chamber pressure, and σ is the variable properties factor defined as

$$\sigma = \frac{1}{[\frac{1}{2}\frac{T_w}{T_0}(1 + \frac{\gamma-1}{2}M^2) + \frac{1}{2}]^{(0.8-\frac{m}{5})}(1 + \frac{\gamma-1}{2}M^2)^{\frac{m}{5}}} \tag{2.15}$$

for diatomic gases $m = 0.6$, Eq(2.16) becomes

$$\sigma = \frac{1}{[\frac{1}{2}\frac{T_w}{T_0}(1 + \frac{\gamma-1}{2}M^2) + \frac{1}{2}]^{0.68}(1 + \frac{\gamma-1}{2}M^2)^{0.12}} \tag{2.16}$$

2.3 Heat Flux Gauge

A heat conduction model of the thin-film gauge is shown in Fig 2.3. The basic equation governing unsteady heat conduction in region 1 is

$$\frac{\partial T_1}{\partial t} = \alpha_1 \frac{\partial^2 T_1}{\partial y^2} \tag{2.17}$$

and the similar equation for region 2 is

$$\frac{\partial T_2}{\partial t} = \alpha_2 \frac{\partial^2 T_2}{\partial y^2} \tag{2.18}$$

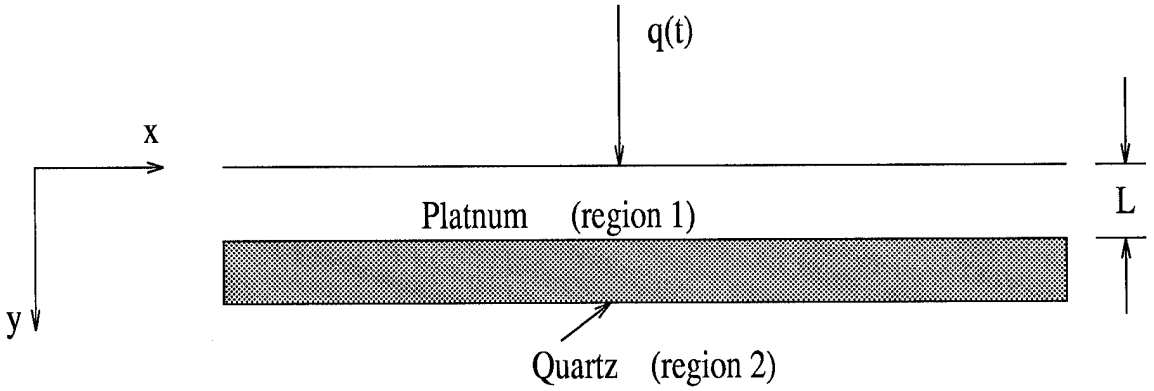

Figure 2.3 Side View of Heat Flux Gauge

The exact solution to the above system of equations with appropriate boundary condition is given by Vidal (15). The exact solution for the surface temperature of a homogeneous body composed only of region 2 is

$$T(t) = \frac{1}{(\pi k \rho c)^{\frac{1}{2}}} \int_0^t \frac{q''(\tau)}{(t-\tau)^{\frac{1}{2}}} d\tau \tag{2.19}$$

For the simple case of a constant rate of heat flux, the surface temperature becomes

$$T(t) = 2q'' \frac{t^{\frac{1}{2}}}{(\pi k \rho c)^{\frac{1}{2}}} \tag{2.20}$$

If q'' is not constant, the realation between the temperature history of the gauge and the heat flux imparted to the surface can be obtained (12)

$$q''(t) = (\frac{\rho ck}{\pi})^{0.5}[\frac{T(t)}{t^{0.5}} + 0.5\int_0^t \frac{T(t) - T(\tau)}{(t-\tau)^{1.5}} d\tau] \tag{2.21}$$

where $(\rho ck)^{0.5}$ is called the thermal product. This form has a singularity at $t = \tau$, so this equation is modified to allow a numerical integration (4).

$$q''(t_n) = (\frac{\rho ck}{\pi})^{0.5}\{\frac{T(t_n)}{t_n^{0.5}} + \sum_{i=1}^{n-1}[\frac{T(t_n)-T(t_i)}{(t_n-t_i)^{0.5}} - \frac{T(t_n)-T(t_{i-1})}{(t_n-t_{i-1})^{0.5}} + 2\frac{T(t_i)-T(t_{i-1})}{(t_n-t_i)^{0.5}(t_n-t_{i-1})^{0.5}}] + \frac{T(t_n)-T(t_{n-1})}{(\Delta t)^{0.5}}\} \tag{2.22}$$

The result can be further simplified by assuming the output of the gauge equals zero when t=0, Equation (2.22) then becomes

$$q''(t_n) = 2(\frac{\rho ck}{\pi})^{0.5}\sum_{i=1}^{n} \frac{T(t_i) - T(t_{i-1})}{(t_n - t_i)^{0.5} + (t_n - t_{i-1})^{0.5}} \tag{2.23}$$

This equation will be used in calculating heat flux.

2.4 Fluid Flow Relations

The governing equations of the isentropic flow of a perfect gas are (1)

$$p = \rho RT \tag{2.24}$$

$$\frac{T_0}{T} = 1 + \frac{\gamma - 1}{2}M^2 \tag{2.25}$$

$$\frac{P_0}{p} = (\frac{T_0}{T})^{\frac{\gamma}{\gamma-1}} \tag{2.26}$$

$$\frac{\rho_0}{\rho} = (\frac{T_0}{T})^{\frac{1}{\gamma-1}} \tag{2.27}$$

For flow through a variable-area duct, the Mach number and area relation can be expressed as

$$(\frac{A}{A_*})^2 = \frac{1}{M^2}[\frac{2}{\gamma+1}(1+\frac{\gamma-1}{2}M^2)]^{\frac{\gamma+1}{\gamma-1}} \tag{2.28}$$

These relations are used to predict flow conditions throughout the nozzle.

2.5 **Porosity**

The nozzle used for the testing was the same nozzle Lenertz (7) used, except the injection area was shrunk to a smaller area between 1.3 cm upstream and 1.2 cm downstream of the throat. A possible equation which relates the pressure drop across the porous wall to the gas velocity through the wall was determined from the porous material flow curve (Fig 2.4) (11).

$$\Delta p = p_{plenum} - p = Au_i^B \tag{2.29}$$

where A and B are constants, p_{plenum} is the plenum pressue and p is the local pressure in the nozzle in the region of porous material.

The local pressure varies along the nozzle. Since the plenum pressure is constant and local pressure is varing, the injection velocity won' be constant. This makes blowing ratio difficult to find. A method to calculate the blowing atio is to divide the whole porous region into several smaller regions. Each region was assumed to have a constant local pressure, p. Therefore the total injected mass flow rate per

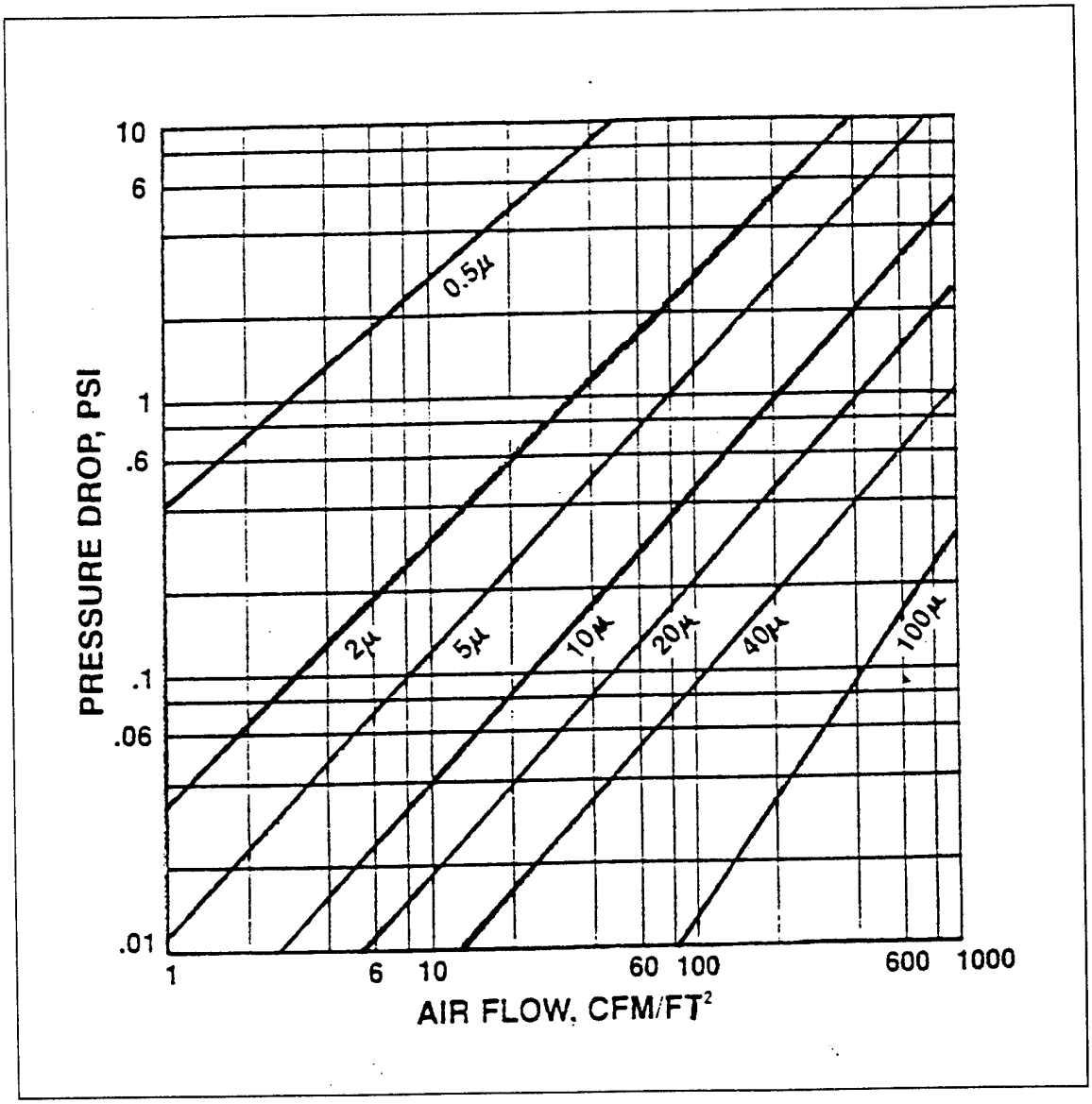

Figure 2.4 Porous Material Flow Curve

area can be obtained by the summation of the local injected mass flow rates divided by injected area.

$$\frac{\dot{m}_i}{A_i} = \rho_i u_i = \frac{1}{A_i} \sum_{j=1}^{N} \rho_i (u_i)_j (A_i)_j \tag{2.30}$$

where $(u_i)_j = (\frac{\Delta p_j}{A})^{\frac{1}{B}}$, N is the number of smaller regions and j is the specific small region number. The primary flow mass flow rate per area can be obtained at the nozzle throat as:

$$\frac{\dot{m}_p}{A_p} = \rho_p u_p \tag{2.31}$$

Equations (2.30) and (2.31) were used in Equation (1.2) to obtain the blowing ratio.

The local pressure drops $(\Delta p)_j$ may be all positive (blowing), all negative (suction), or part positive and part negative depending on the value of plenum pressure. If the local pressure drops are all positive or negative, the velocities of injection will be all positive or negative. These velocities will be multiplied by the injected fluid density and added together to determine the blowing ratio. If the situation happens to have part negative pressure drops and part positive pressure drop, only the region of positive pressure drop will be considered in determining the blowing ratio.

III. EXPERIMENTAL APPARATUS AND PROCEDURE

3.1 Calibration

3.1.1 **Pressure Transducer.** The Endevco Model 8530A-100 pressure transducers were calibrated by using an AMETEK Model HK-500 Pneumatic Pressure Tester. Each transducer was calibrated with its associated shielded cable and Endevco Model 4423 signal conditioner attached as in experimental measurements. The pressure transducer output was recorded for eleven pressures and amplified using a Model 4423 signal conditioner. The output from the signal conditioner was read by an HP Model 3466A Digital Voltmeter as a function of the input gauge pressure in pound per square inch. The data points for each transducer were ploted with linear least square fits in Appendix A.

3.1.2 **Thin-film Heat Flux Gauge.** Two kinds of calibration were needed. They are static calibration and dynamic calibration. Static calibration involved finding the steady-state conversion factor from voltage to temperature. Dynamic calibration attempted to find the thermal product $\sqrt{\rho ck}$ of the heat flux gauge. For the static calibration, the heat flux gauges and a thermocouple were placed into a holder(see Figure 3.1) covered with a protective sheet of thin latex. The holder was adjusted in height and set into a beaker of water. A shielded cable connected the three heat flux gauges to three Transamerica PSC 8115 Wheatstone bridge modules. Three PSC 8015 Amplifiers supplied a constant 2.5V DC to the Wheatstone bridge modules. The heat flux gauge acts as one leg of the initially balanced bridge. Once the temperature of the gauge changes, the bridge becomes unbalanced and a voltage output was created from the bridge. The bridge output voltage was amplified and

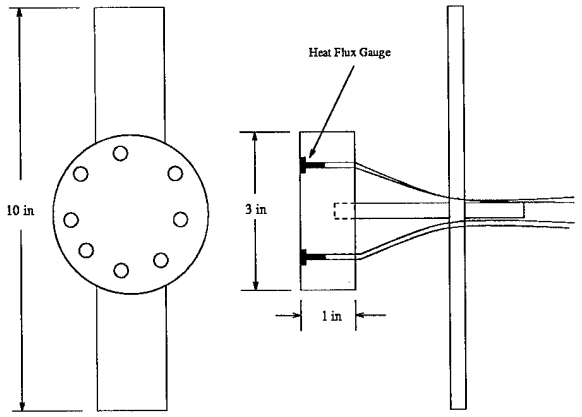

Figure 3.1 Heat Flux Gauge and Thermocouple Holder

filtered by the programmable PSC 8015-1 amplifier before being fed into the Nicolet 500 Data Acquisition System(see Fig 3.2)

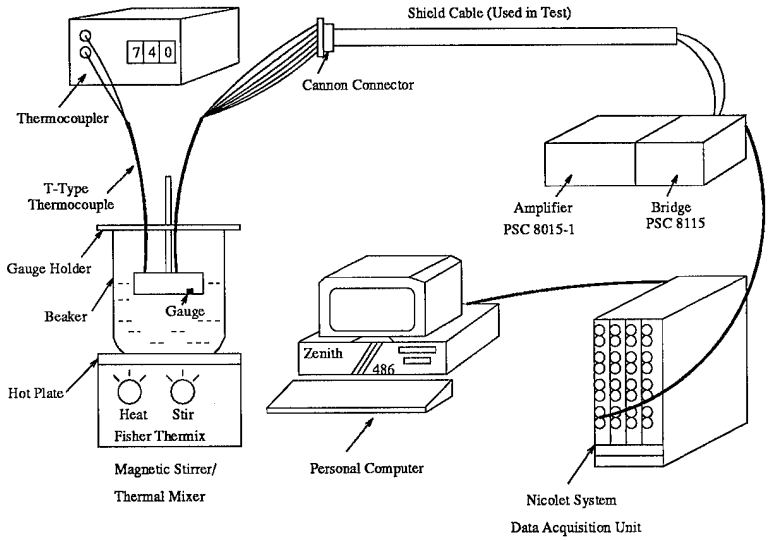

Figure 3.2 Heat Flux Gauge Static Calibration Apparatus

The water temperature was varied from 23.5°C to 39.4°C. Ten temperature points vs. the output of bridges were taken and plotted with linear least square (see Appendix B).

The dynamic calibration was more complex. The heat flux gauges were installed into an existing flat plate which was modified to hold eight heat flux gauges aligned perpendicular to the flow (see Fig 3.3). All gauges were assumed to be exposed to the same value of heat flux in the shock tube. The gauge temperature plots were forced to yield the same value of heat flux from Eq(2.23) and Eq(2.10) by varying the thermal product value.

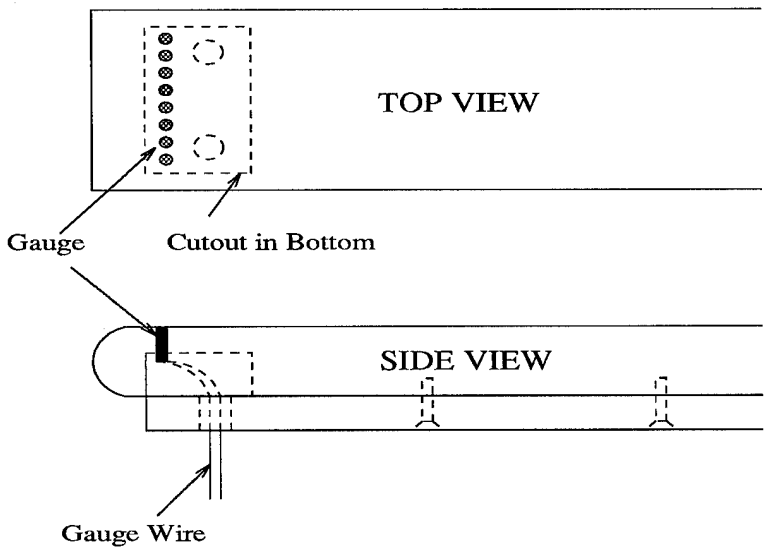

Figure 3.3 Flat Plate with Heat Flux Gauges

Five sets of data for each gauge were recorded using 435.9 kPa air in the shock tube driver section. These data were input into a program called FLTPLT (7) which computed the heat flux and heat transfer coefficient at the gauge for one particular flow condition.

To find the thermal product of the gauges, one gauge was first assumed to have a known thermal product ($\sqrt{\rho ck} = 1520$). Then the thermal product of the other two gauges were varied until the value of heat flux and heat transfer coefficient were all the same. The results are shown in Table 3.1.

$GaugeSerialNumber$	$S/N48$	$S/N58$	$S/N530$
Heat Flux (W/m^2) q''	83424.6	83420.4	83424.8
Deviation (W/m^2) σ	630.333	665.010	859.122
Heat Coefficient (W/m^2K) h	1175.28	1175.26	1171.96
Deviation (W/m^2K) σ	9.01	12.31	9.6
Thermal Product $(J/m^2Ksec^{0.5})$ $\sqrt{\rho c_p k}$	1520	1430.77	1632
Deviation $(J/m^2Ksec^{0.5})$ σ	0	14.33	9.9

Table 3.1 The Result of Heat Flux Gauge Calibration

3.2 Shock Tube

The facility used for this experiment was the AFIT low speed shock tube located in room 146 of building 640. The shock tube is 20.32 cm (8 in) tall, 10.16 cm (4 in) wide, and has a 1.22 m (4 ft) long driver section, a 4.88 m (16 ft) driven section and a 1.22 m (4 ft) test section. A 0.18 mm (0.007 in) thick mylar diaphragm was used to separate the high-pressure driver section from the low-pressure driven section (see Fig 3.4).

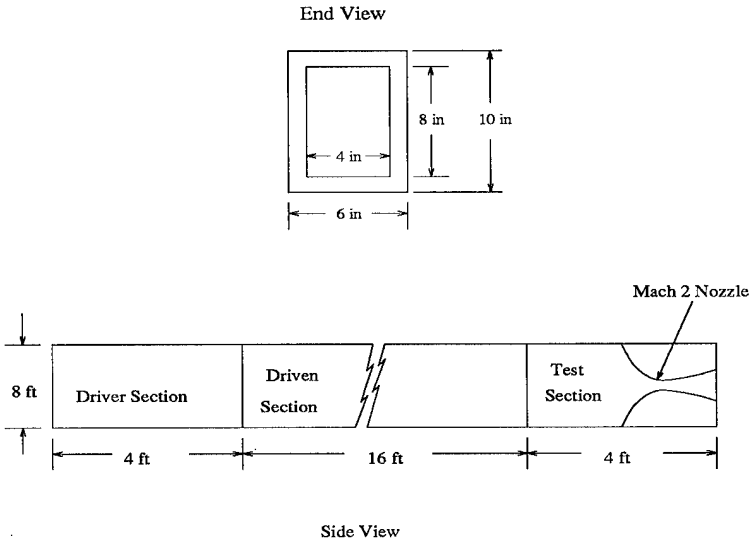

Figure 3.4 Shock Tube Apparatus

The simulated combuster chamber conditions used to find the actual stagnation temperature were obtained from Eqs (2.1) through (2.9) by assuming the shock wave reflected from a straight wall.

3.3 Mach 2 Nozzle

The test model in this experiment was a two dimensional, converging diverging nozzle located at the end of the shock tube (see Fig 3.4). The design of the size and shape of the nozzle was discussed in Lenertz thesis (7).

Fig 3.5 shows the nozzle configuration. The nonblowing side (top) of the nozzle had a 7.6 cm (3 in) circular cavity and twin instrumentation channels hollowed out to allow installation of one flux gauge and three pressure transducers. A heat flux gauge was placed 5.5 mm (0.22 in) downstream of the throat. The Mach number at this position was M=1.17. Three pressure transducer were placed 4.2 cm (1.657 in) prior to and 5.5 mm (0.22 in), 3.1 cm (1.22 in) downstream of the throat. The stagnation pressure was measured by a pressure transducer which was installed prior to the throat.

The gas supply cavity in the blowing side was 7.7 by 7.6 cm square and was drilled completely through the nozzle wall from the bottom. A shelf was cut 6.4 cm (1/4 in) deep on the top of the cavity. This allowed four layers of 1.59 mm (0.0625 in) thick porous plate to fit onto the shelf and be level with the inner wall of the nozzle. The first layer was all porous material which was 316L stainless steel with a 2 micron pore size. The second to fourth layers were porous material from a point 1.3 cm (0.551 in) before the throat to 1.2 cm (0.467 in) downstream of the throat and solid material from 1.2 cm mm (0.467 in) downstream of the throat to the exit. This limited the injection to a small area near the throat. One heat flux gauge was placed 5.6 mm (0.219 in) downstream of the throat and three pressure transducer were placed 5.6mm (0.219 in), 3.1 cm (1.217 in) and 5.5 cm (2.172 in) downstream of the throat.

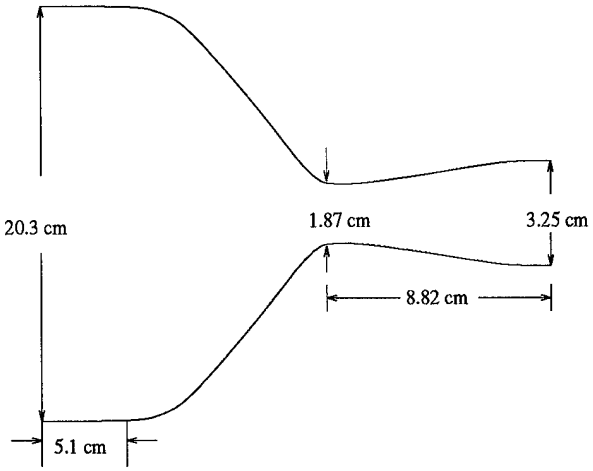

(a) Silhouette View

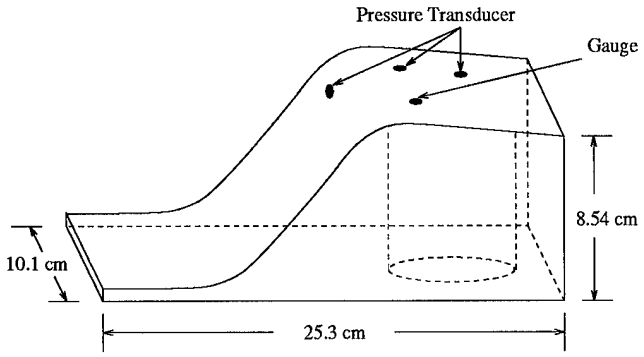

(b) Nonblowing Side View

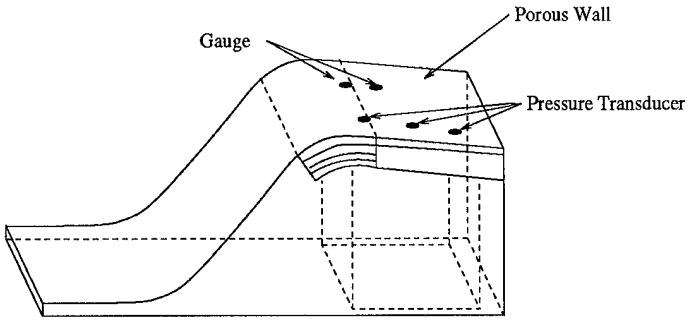

(c) Blowing Side View

Figure 3.5 Nozzle Configuration

3.4 Data Collection

An instrumentation diagram is shown in Fig 3.6 in which heat flux gauges and pressure transducers were used to sense temperature and pressure change respectively via voltage changes. These voltage changes were amplified and fed into a Nicolet 500 System which was used to record the output.

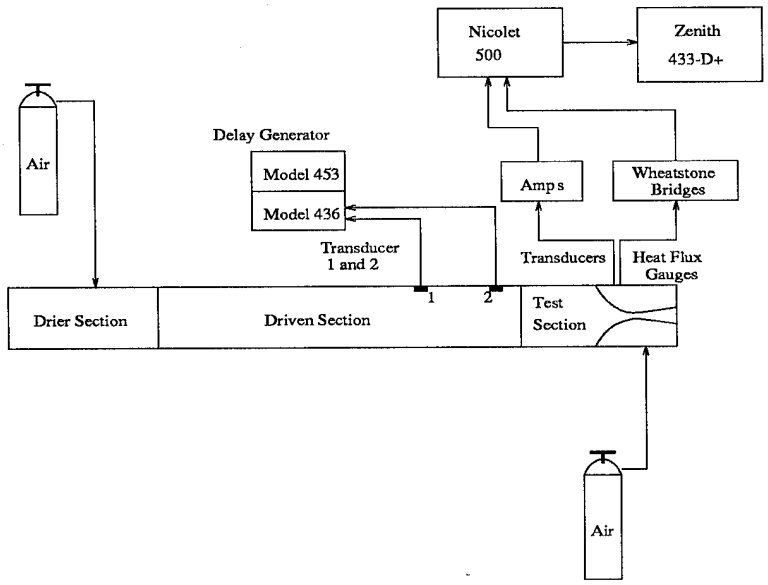

Figure 3.6 Instrumentation Diagram

Before each test, the Wheatstone bridges were balanced. This ensured the heat flux gauge and pressure transducers had a zero output at ambient condition. The Nicolet 500 System was configured, the air used to supply transpiration cooling was set to a desired level, and the shock tube was flushed with dry air for 5 minutes to avoid the variable hunidity associated with room air.

After recording the ambient and plenum pressure and temperature, a mylar diaphragm was installed in the shock tube, the Nicolet 500 System was enabled, and the driver section of the shock tube was pressurized. Just before the driver section pressure reached the desired value, the valve controlling the injection air was opened. When the diaphragm in the shock tube was ruptured, a shock wave was

propagated along the shock tube and triggered two pressure transducers on the top of the shock tube. The time for the shock wave to travel between these two pressure transducers was measured. The shock wave also triggered the heat flux gauges and pressure transducers in the nozzle, and data behind the shock wave were recorded by the Nicolet 500 System and transferred to files in the Zenith 433 D+ Computer. Because the data obtained were in binary code form, they were converted into ASCII code form for later manipulation.

3.5 Shadowgraph Flow Visualization System

A shadowgraph system contains three basic items: an aperature, light source and a mirror shown in Fig 3.7. The light source, the mirror and desired image should be at the same height to ensure that the light passed perpendicularly through the flow.

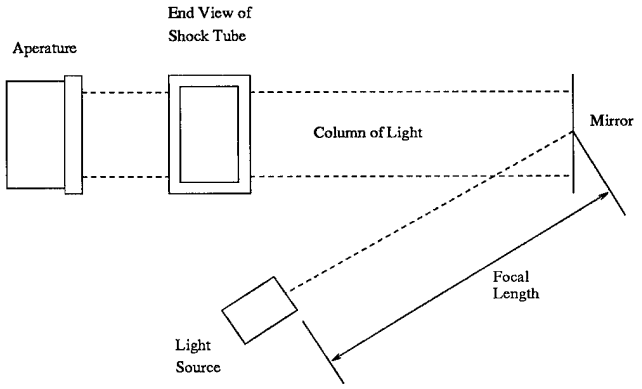

Figure 3.7 Shadowgraph Configuration

A light was triggered and transmitted to a mirror which has a focal length from the light source, and reflected from the mirror in an uniform column through the flow being photographed and exposed film. Because the desired time to expose the film was very short, it was very difficult to trigger the light source by hand. An electrical system, Cordin Model 435 Proportional Delay Generator and Model 453

Delay Generator, was employed to trigger the light source (Xenon 10 nsec Lamp) at a preset time measured in microseconds after the shock wave passed the second shock tube pressure transducer.

IV. RESULTS AND DISCUSSION

4.1 Test Condition

A table for the actual test condition is listed below.

P_1	99.1 kPa
P_4	590.2 kPa
P_5	413.8 kPa
T_5	458.0 K
P_0	376.9 kPa
T_0	445.8 K
W	484.8 m/sec

Table 4.1 Summary of Test Condition

where P_4 was the driver pressure, P_1 was the driven pressure, P_5 and T_5 were the simulated combustion chamber pressure and temperature respectively obtained from Eq(2.5) through (2.9) with The given shock wave speed, P_0, T_0 were the actual stagnation pressure and temperature respectively, and W was the measured shock wave speed.

It was noticed that the real stagnation pressure is less than the theoretical stagnation pressure. This is because the shock wave was reflecting from a converging nozzle section instead of a straight wall. Fig 4.1 shows the pressure profile measured from the pressure transducer located 4.2 cm prior to the nozzle throat. The actual stagnation pressure P_0 was picked and averaged between 2.5 ms and 3 ms and its value was 376.96 kPa. The actual stagnation temperation was obtained by substituting the theoretical stagnation pressure P_5, theoretical stagnation temperature T_5, actual stagnation pressure P_0 into Eq(2.26), and its value was 445.82 K.

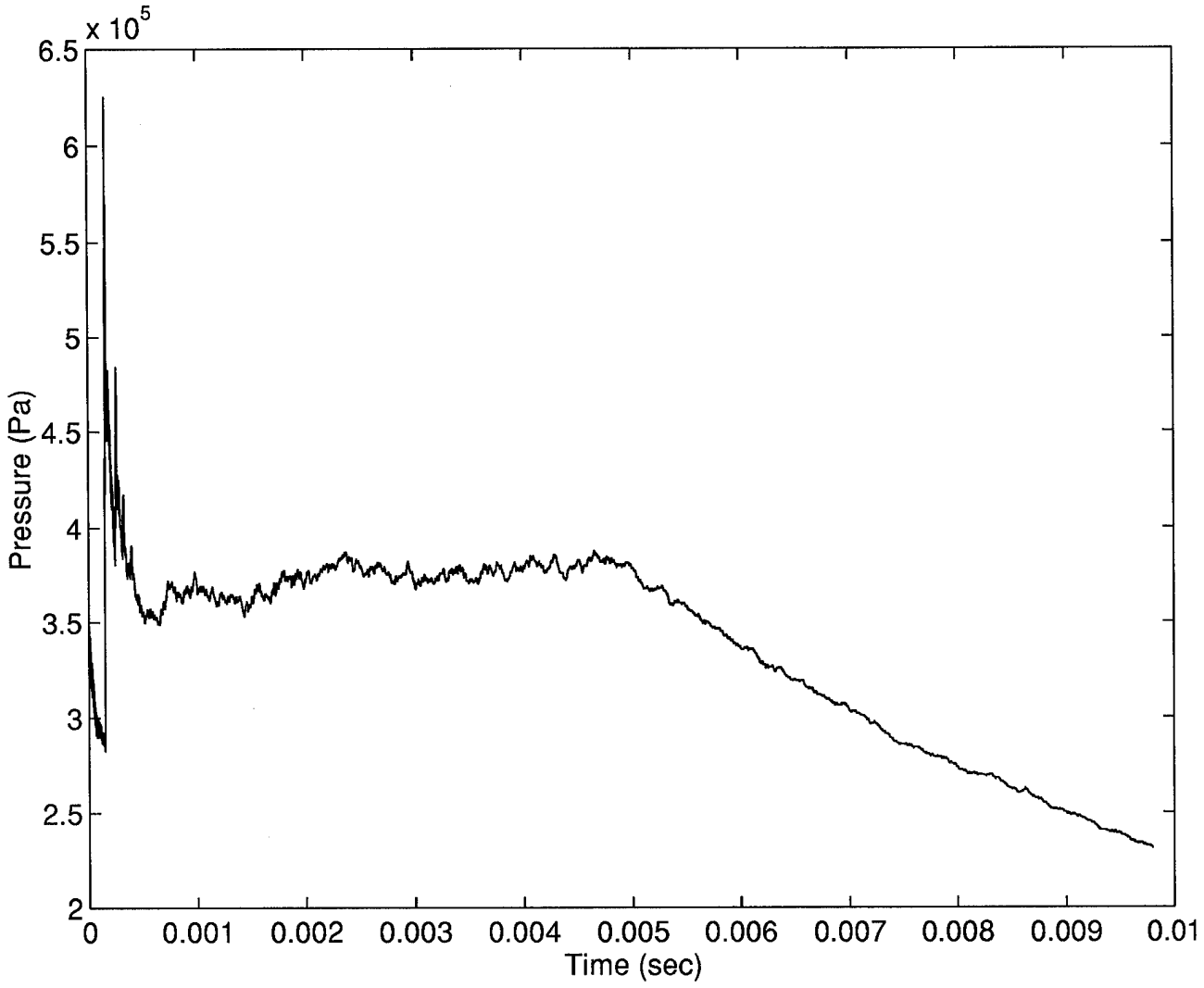

Figure 4.1 The Chamber Pressure History

4.2 Static Pressure Distribution

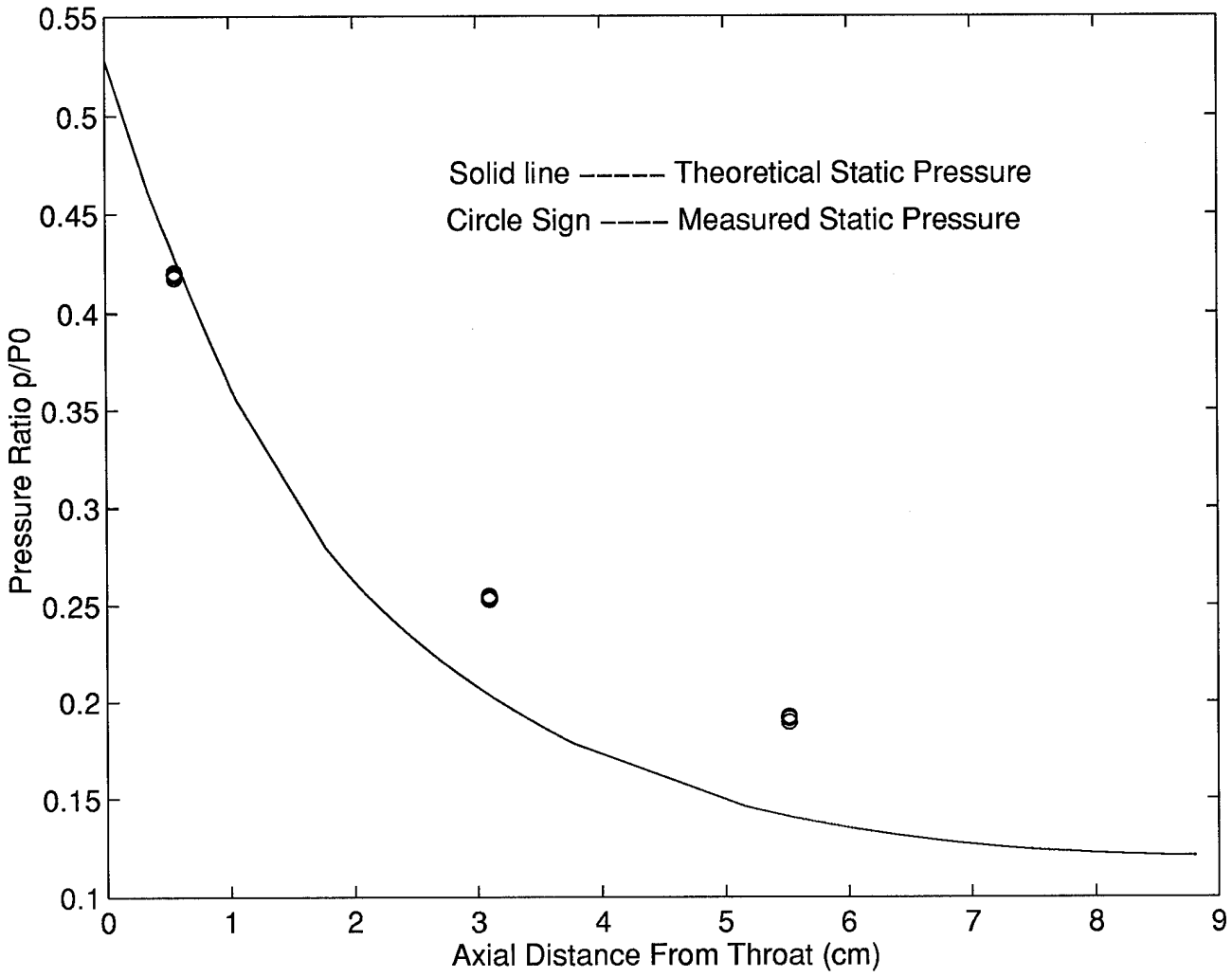

Figure 4.2 Ratio of Static to Stagnation Pressure Along the Nozzle

The theoretical static pressure distribution along the nozzle for the reference case of no injection was compared to the measured pressure distribution. It is given in Fig 4.2.

Both the measured and theoretical static pressures have been normalized by the total pressure at the combustion chamber. It is seen that very good agreement is obtained at the location near to the throat, but there is a disagreement at the locations far downstream of the nozzle throat. This deviation was most likely caused by the friction, taper and curvature of the nozzle.

In addition, the influence of blowing on the static pressure at three specified locations was investigated. Those locations were 0.56 cm, 3.09 cm, and 5.52 cm downstream of the nozzle throat. The pressure ratio vs the blowing ratio for three different locations were plotted in Fig 4.3. In Fig 4.3a, The static pressure increased 13.8% with an increase of the blowing ratio to 0.012. This increased pressure was due to the flow energy loss which was spent to accelerate the low velocity injected air. In Fig 4.3b and 4.3c, the static pressure downstream of the blowing region wasn't influenced by the increasing blowing ratio. This result is in good agreement with Azevedo (2) in which the static pressure appears to be more sensitive to plenum pressure as the injection angle is raised.

4.3 Exit Mach Number

In this section, the exit Mach numbers for different blowing ratios were measured. Fig 4.4 shows the exit Mach number vs blowing ratio measured at the centerline of the nozzle and 0.32 cm above and below the centerline respectively. These results showed that transpiration limited to the region of the nozzle throat did not affect the exit Mach number distribution, since the flow was mixed together with the injected air downstream of the blowing region, and also showed that the effect of transpiration was limited to the region where the injected air enters the boundary layer. This was verified by shadowgraph photographs taken for each blowing level. From Fig 4.5, it can be seen that the boundary layer thickness on the blowing side (bottom side) was unchanged with increasing blowing.

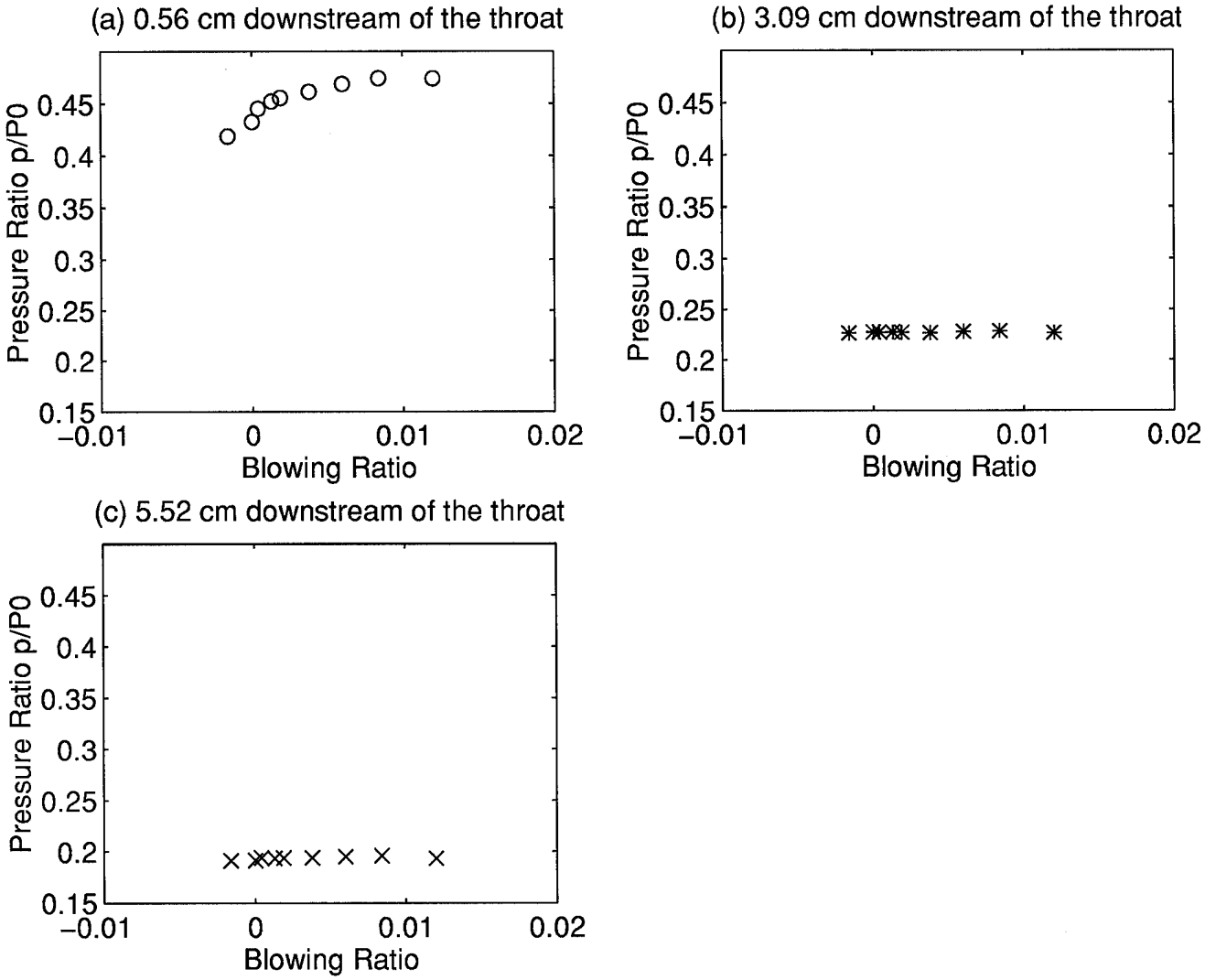

Figure 4.3 The Influence of Blowing on the Static Pressure at Three Specified Locations with $P_0 = 377kPa$

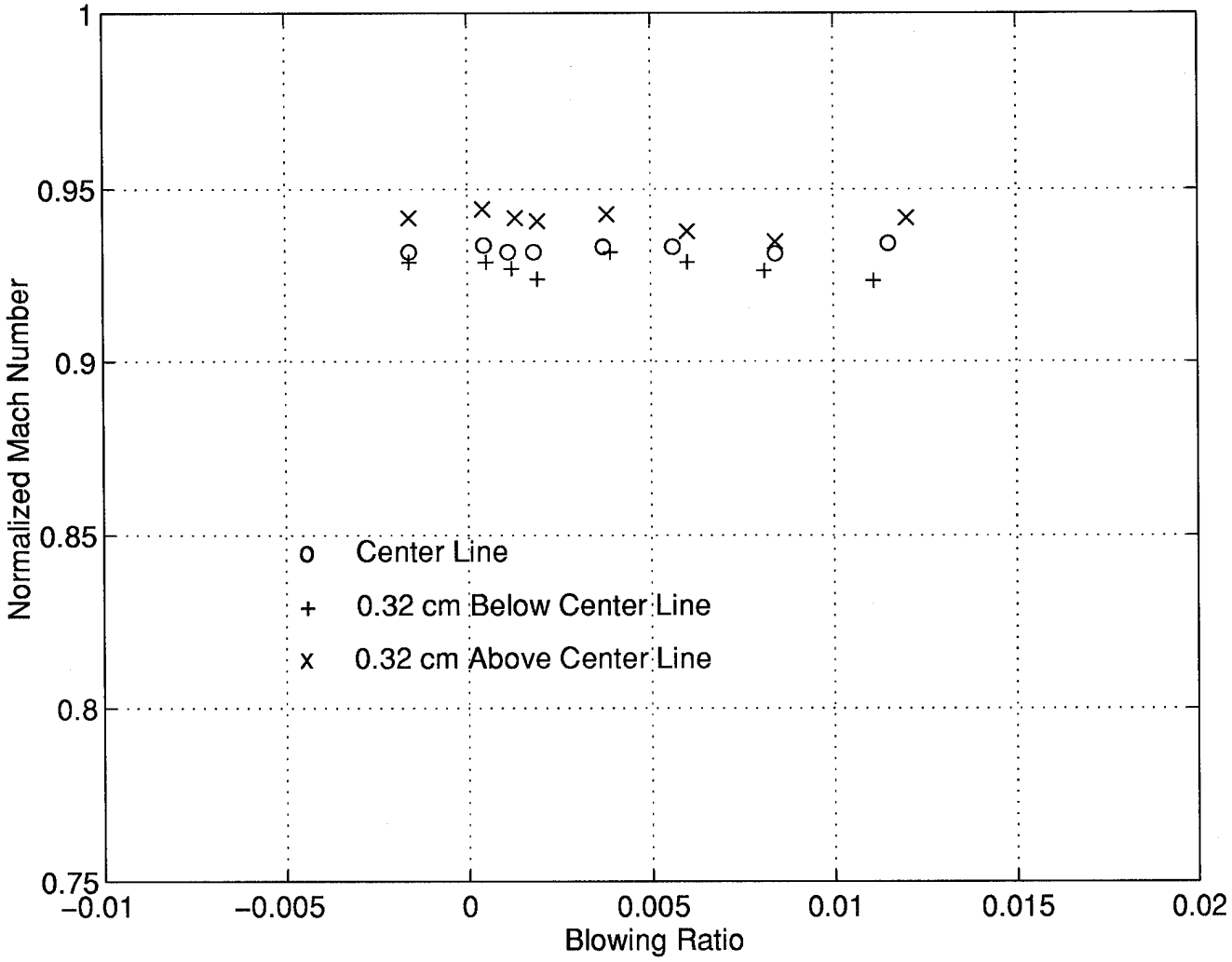

Figure 4.4 Normalized Mach Number Versus Blowing Ratio, Uncertainty=1%

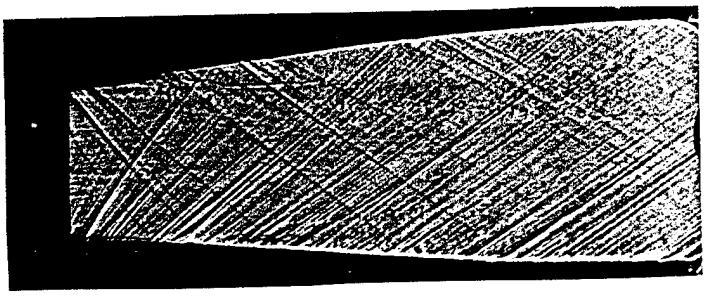

(a) Blowing Ratio BR=0.

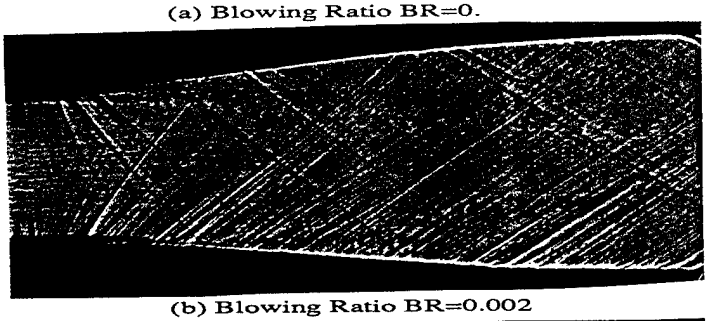

(b) Blowing Ratio BR=0.002

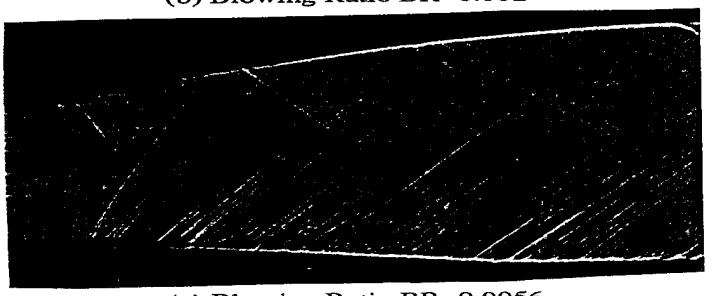

(c) Blowing Ratio BR=0.0056

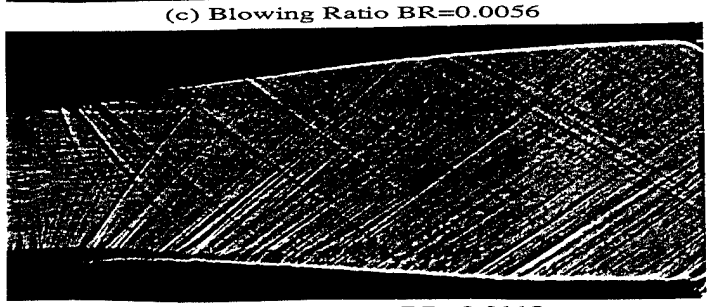

(d) Blowing Ratio BR=0.0112

Figure 4.5 Shadowgraph Showing Boundary Layer at Each Blowing Level

4.4 Heat Transfer Result

4.4.1 **Uncooled Heat Flux Coefficient.** A predicted uncooled heat transfer coefficient along the nozzle, obtained from Eq (2.14), is shown in Fig 4.6. It is compared with the experimental data (Table 4.2) measured from the nonblowing side and blowing side 5.6 mm downstream of the nozzle throat.

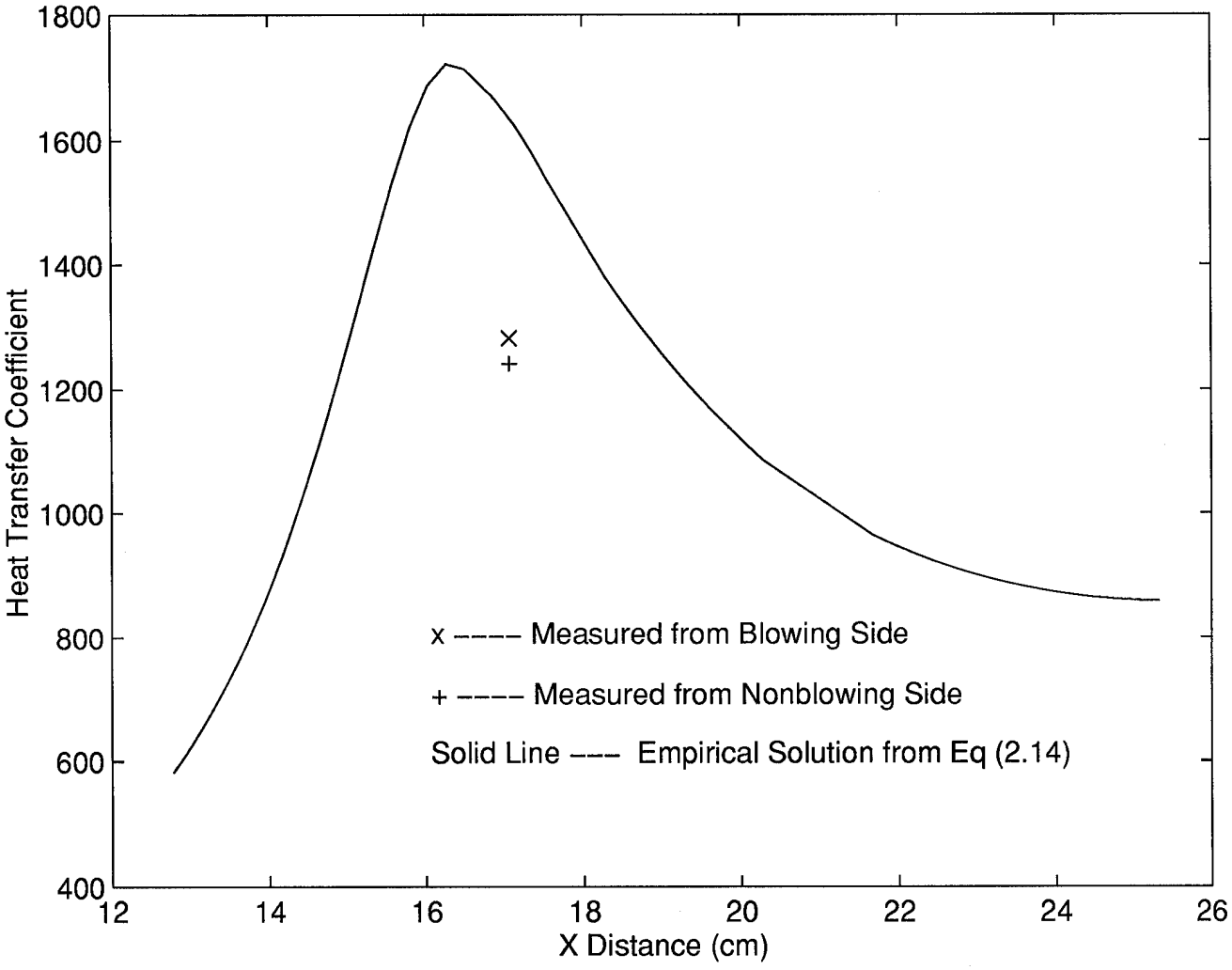

Figure 4.6 Measured and Predicted Heat Flux Coefficient Without Blowing

Gauge Serial Number	S/N 48 (Blowing Side)	S/N 58 (Nonblowing Side)
h (W/m^2K)	1273.7	1244.3
	1304.5	1265.4
	1262.3	1214.3
	1288.2	1240.7
Average (W/m^2K)	1282.2	1241.2
Deviation (W/m^2K)	18.28	20.97

Table 4.2 Nonblowing Heat Transfer Coefficient

The errors between the prediction and measurement on nonblowing and blowing side were 24.16 % and 21.66 % respectively. Welsh and Witt (16) presented a comparison between experimental data and the theoretical prediction of Bartz (3) for nozzles with different geometries and found the prediction of Bartz were overestimated for a nozzle with an 8 to 1 contraction-area ratio and underestimated for a 1.64 contraction-area ratio nozzle in the peak values of the heat flux. Since the contraction-area ratio for the nozzle used in these tests was 10.87 to 1, it seemed to explain why the prediction of Bartz overestimated the present data.

4.4.2 **Effect of Transpiration Cooling.** In order to evaluate the effectiveness of transpiration cooling, the noninjection heat transfer was required for comparison. Four groups of data were evaluated. Two of them were evaluated in the range of -0.0016 to 0.0038 blowing ratio and the rest were evaluated in the range of -0.0016 to 0.0117 blowing ratio. The results shows a general trend toward increased cooling as the blowing ratio increases. Fig 4.7 depicts heat transfer as the ratio of measured heat transfer coefficient to measured nonblowing heat transfer coefficient vs blowing ratio, and the result from Lenertz thesis (dashed line and sign) (7).

The negative blowing ratio in Fig 4.7 resulted from the condition where the plenum pressure was lower than the primary flow pressure everywhere along the nozzle in the region of blowing. Once the plenum pressure is higher than the primary flow pressure at any point in the region of blowing, the blowing ratio will have a

positive value. Since for a negative blowing ratio, the heat transfer coefficient was higher than for zero blowing, this is not of concern in transpiration cooling. However a positive blowing resulted in about 40% reduction in heat transfer at the maximum tested blowing ratio of 0.0117.

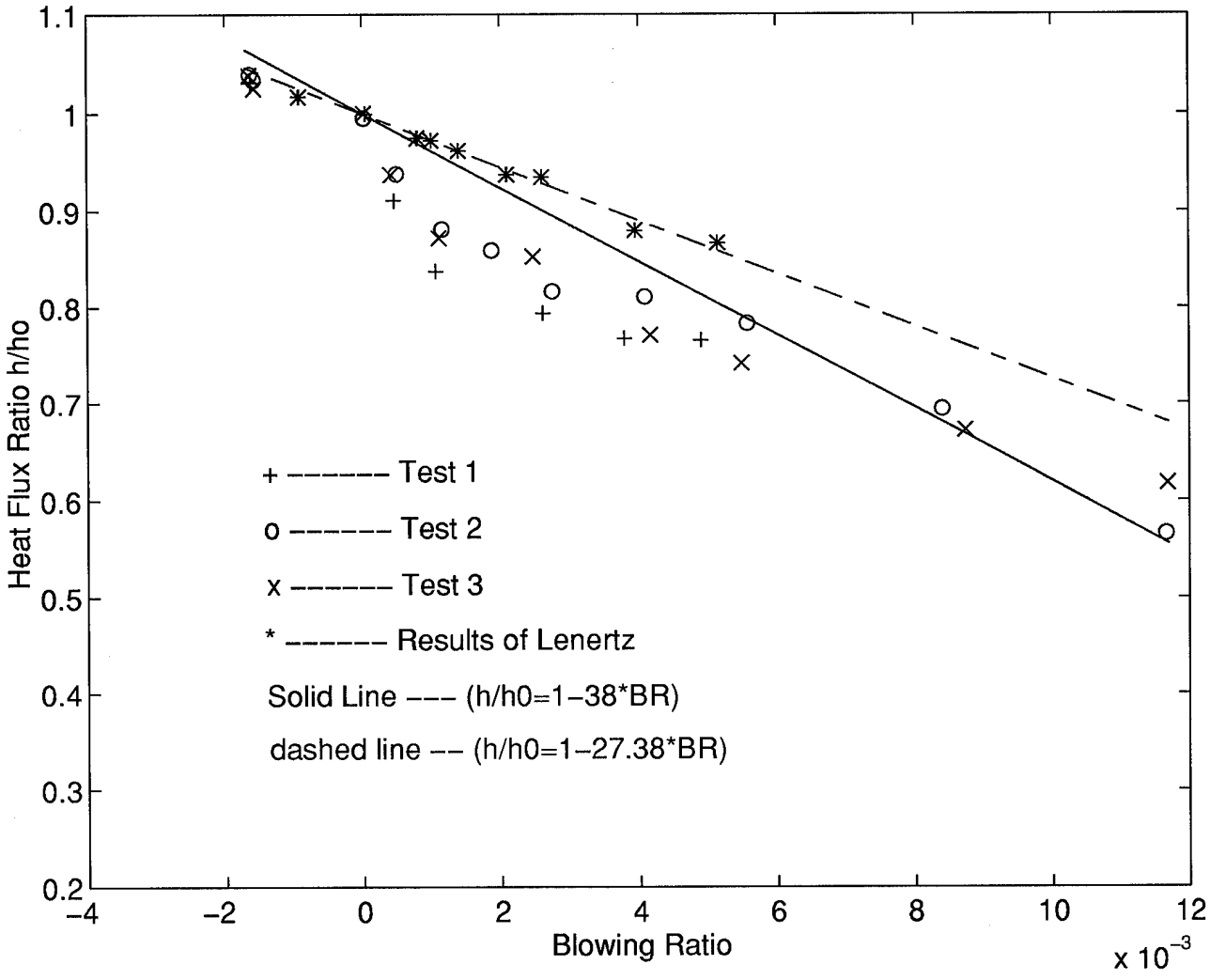

Figure 4.7 Effectiveness of Transpiration Cooling in Mach 2 Nozzle, Uncertainty=9%

A curvefitting for these data from zero blowing ratio to blowing ratio 0.0117 was obtained and can be expressed as

$$\frac{h}{h_0} = (1 - 38 \times BR) \tag{4.1}$$

V. CONCLUSIONS AND RECOMMENDATIONS

5.1 Conclusions

An experimental method has been applied to determine the effectiveness of transpiration. The coolant air was injected at various rates through a porous region between 1.3 cm upstream and 1.2 cm downstream of the nozzle throat.

At the two locations where measurements were made, the heat transfer for zero injection predicted by Eq (2.14) over estimated the experimental data. For positive injection, the experiments present a linear relation between heat transfer coefficient and blowing ratio. Heat transfer coefficient was reduced by about 40% at the blowing ratio BR=0.0117.

For the analysis of the downstream effects, it was found that the exit Mach number at the nozzle center line, 0.32 cm above and below the center line were unchanged with the increasing blowing ratio. Also, from visualization of the shadowgraph, the boundary layer thickness remain unchanged with the blowing ratio increases. This result shows a good improvement compared to the result obtained by Keener (6).

5.2 Recommendations

Three recommendations for future research are made.

First, although this research was focused on the effect of transpiration in the region near the nozzle throat, information about the effectiveness of transpiration at locations downstream of the injected region would be needed. Unfortunitely, due to the lack of the heat flux gauges (only three heat flux gauges were installed in the

nozzle), the effectiveness of transpiration downstream of the injected region was not acquired during the test.

Second, it is seen that the plenum pressure can be increased by shrinking the injected area; but, the injected velocity are still limited by the small porous size. Therefore, a bigger size porous material is recommended for use in future research to obtain larger blowing ratios.

Third, most rocket engines are cooled by regenerative cooling by pumping a liquid through channels surrounding the outside of the combustion chamber walls and the nozzle walls. Since liquid is the main coolant in a rocket engine, evaporative cooling or a combination of evaporative and transpiration cooling is recommended for future research.

Appendix A

The location and number of each pressure transducer is shown in Fig $A.1$,

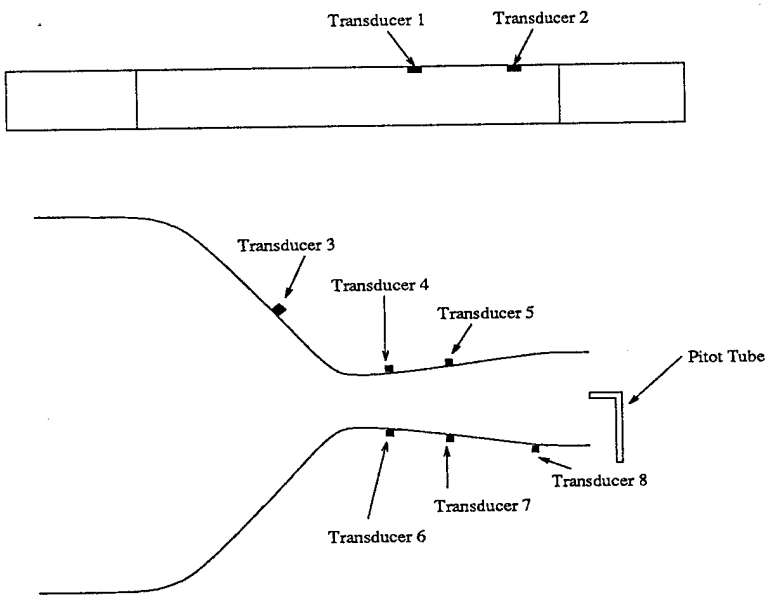

Figure A.1 Location of Pressure Transpiration in the Nozzle and Shock Tube

where transducer 1 and 2 were 0.88 m apart were used to measure the shock wave velocity. Transducer 3 which was 4.2 cm prior to the throat was used to measure the chamber pressure. Transducers 4, 6 and 5, 7 which were 5.5 mm and 3.1 cm downstream of the throat respectively, and transducer 8 which was 5.5 cm downstream of the throat were used to measure the static pressure. The pitot tube was used to measure the stagnation pressure at the nozzle exit.

Each transducer was calibrated before the experiment. The results of the calibration are shown in Figs $A.2$ through $A.10$, and the equations of the least square fit for these calibration were listed below.

Transducer Number	Serial Number	Linear Relation
No.1	S/N WB80	$p = \frac{(v+0.011885)}{9.319029 \times 10^{-6}}$
No.2	S/N 44AM	$p = \frac{(v+0.011449)}{8.384144 \times 10^{-6}}$
No.3	S/N TN05	$p = \frac{(v+0.011295)}{8.044218 \times 10^{-6}}$
No.4	S/N TM73	$p = \frac{(v+0.010603)}{9.761749 \times 10^{-6}}$
No.5	S/N 29BA	$p = \frac{(v+0.005603)}{7.427301 \times 10^{-6}}$
No.6	S/N TM83	$p = \frac{(v+0.009218)}{1.001191 \times 10^{-5}}$
No.7	S/N J82P	$p = \frac{(v+0.001475)}{5.294029 \times 10^{-6}}$
No.8	S/N TN04	$p = \frac{(v+0.00818)}{1.017201 \times 10^{-5}}$
Pitot Tube		$p = \frac{(v+0.012017)}{1.638312 \times 10^{-5}}$

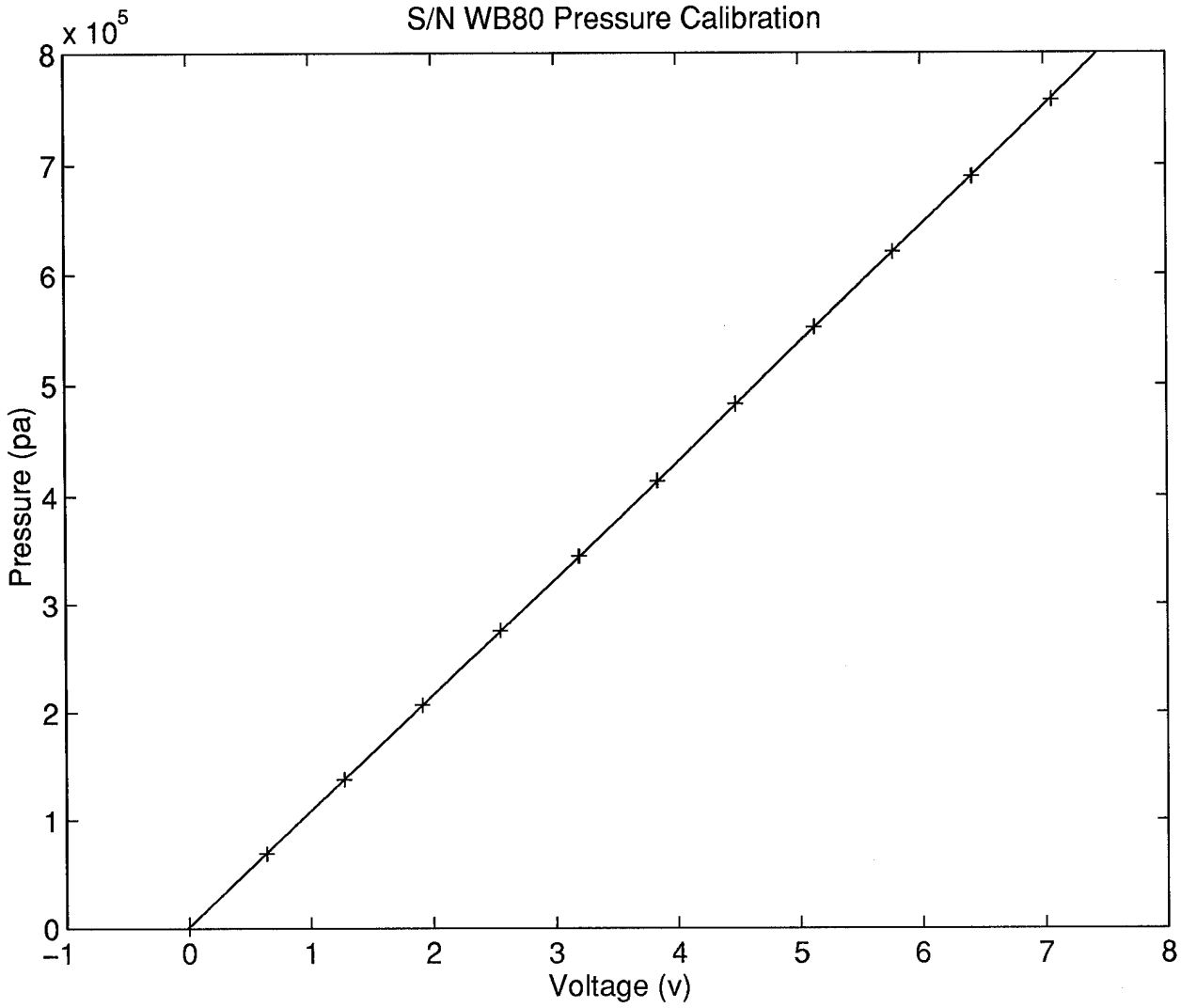

Figure A.2 Calibration For Pressure Transducer No.1

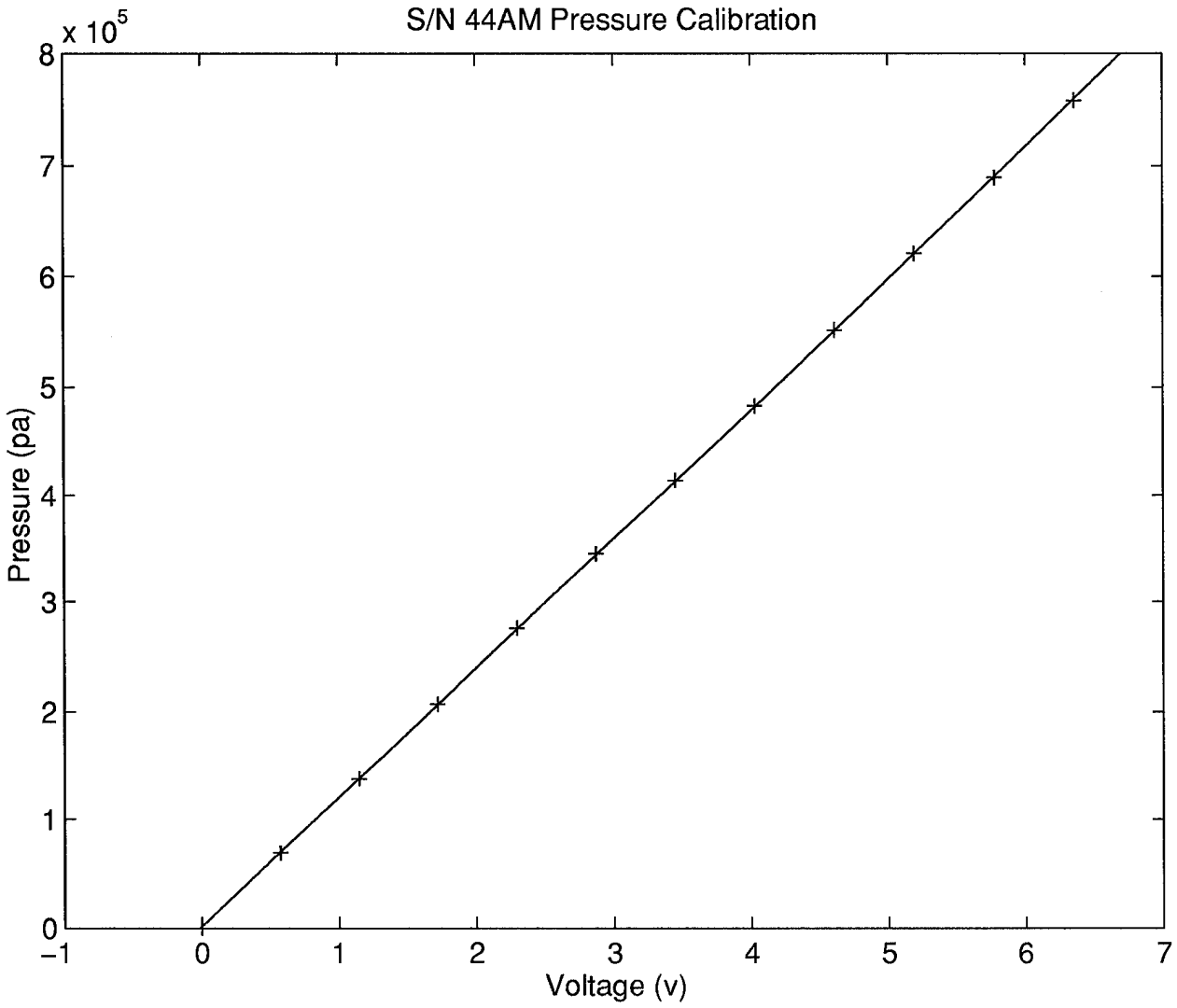

Figure A.3 Calibration For Pressure Transducer No.2

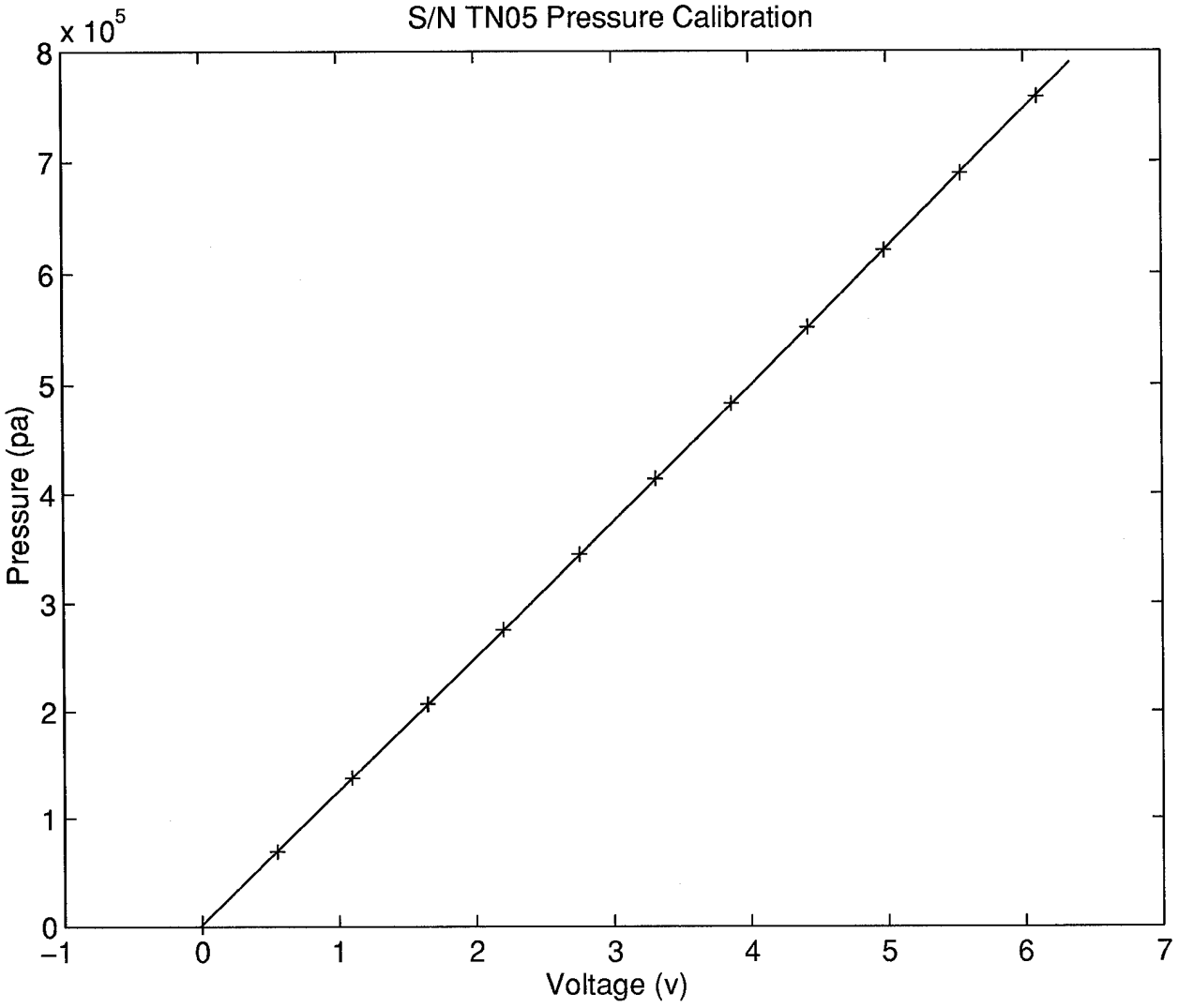

Figure A.4 Calibration For Pressure Transducer No.3

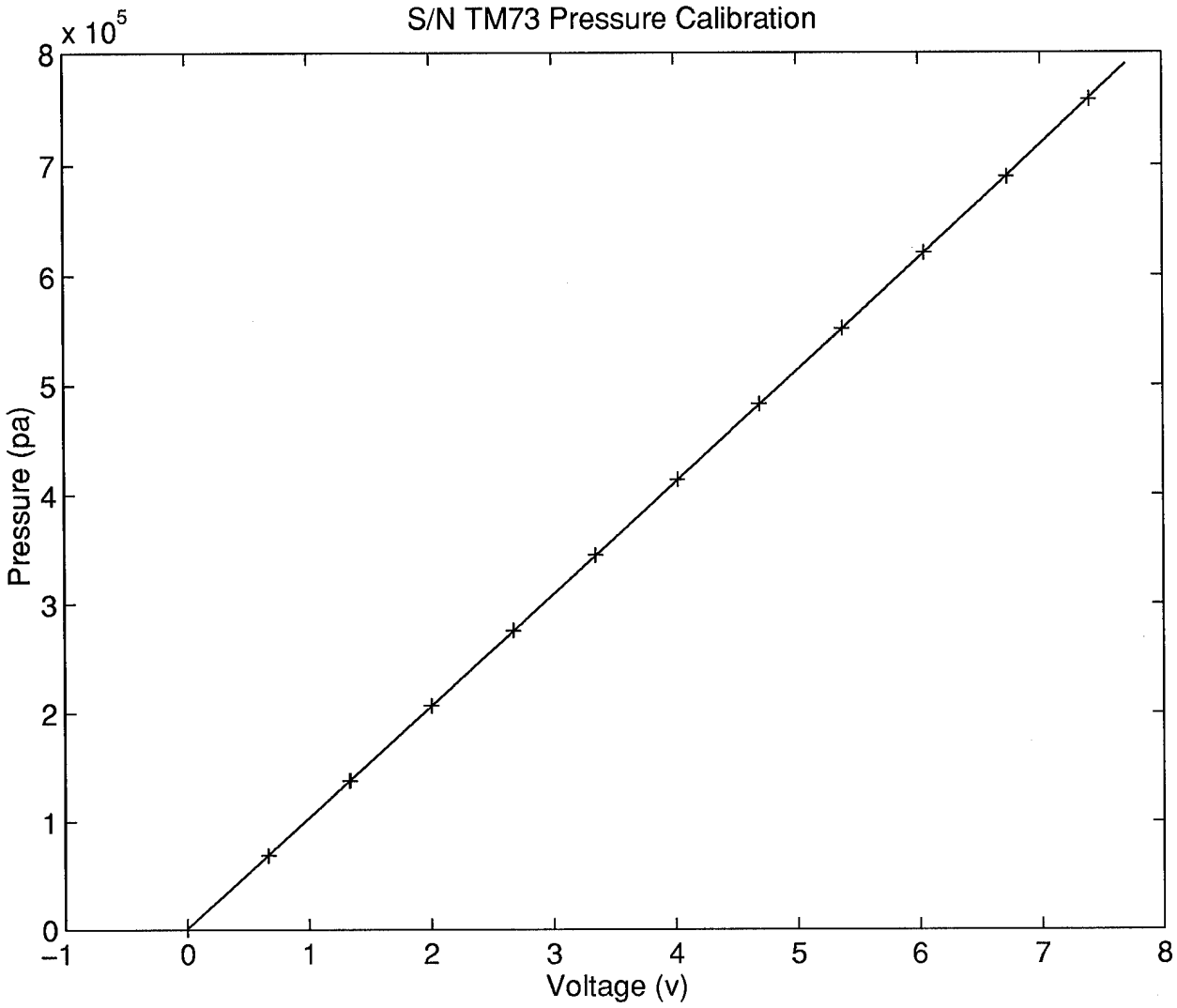

Figure A.5 Calibration For Pressure Transducer No.4

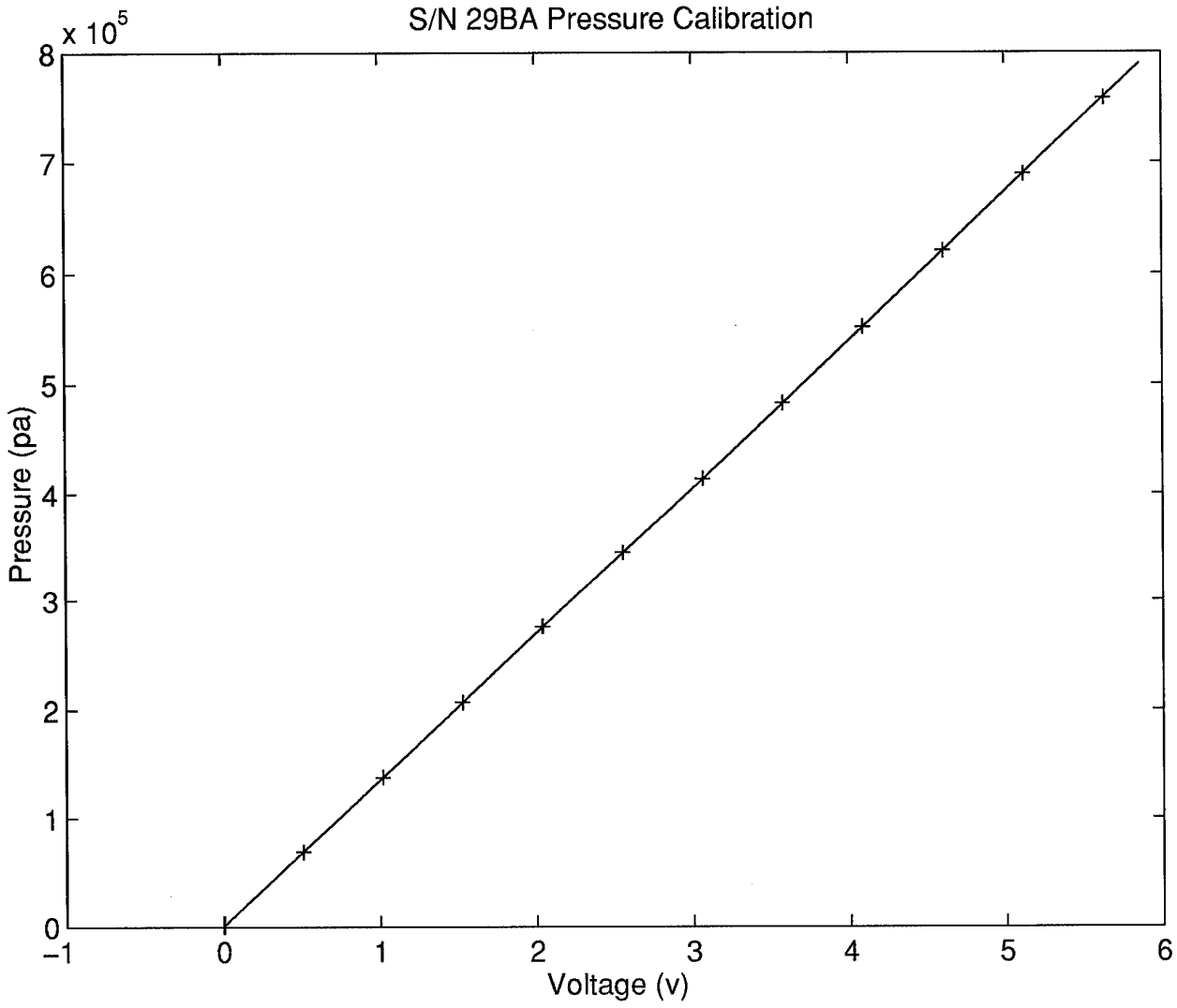

Figure A.6 Calibration For Pressure Transducer No.5

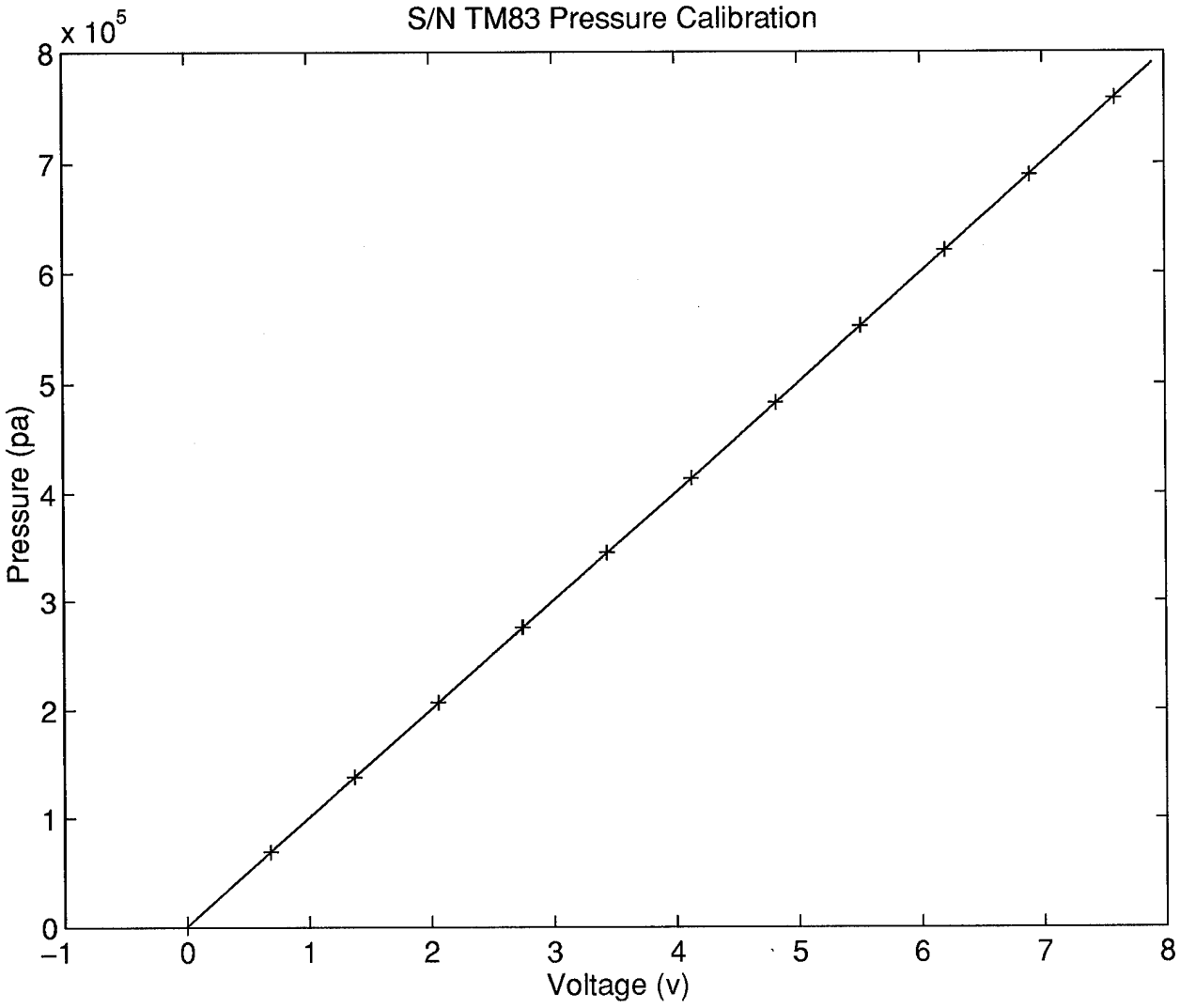

Figure A.7 Calibration For Pressure Transducer No.6

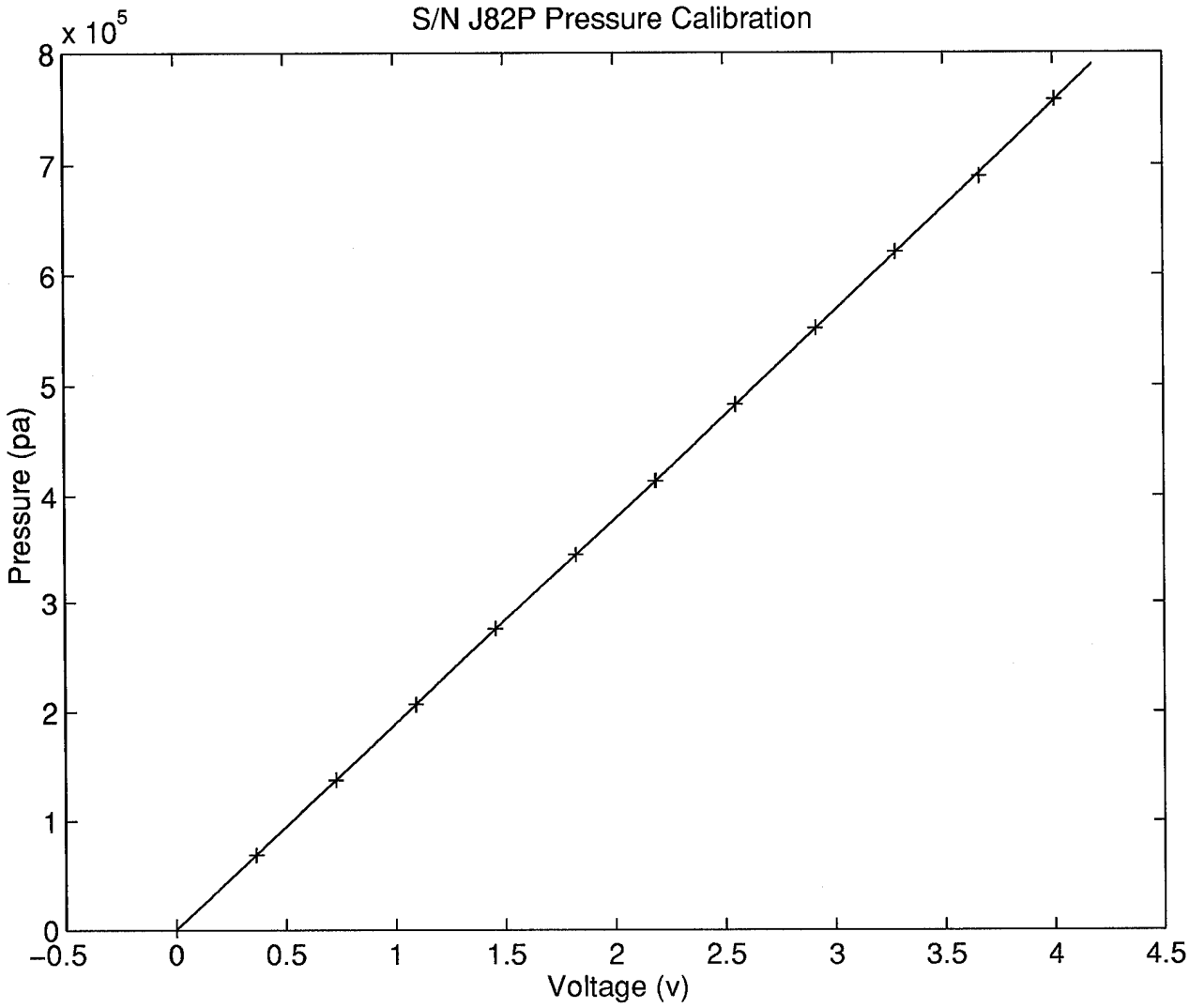

Figure A.8 Calibration For Pressure Transducer No.7

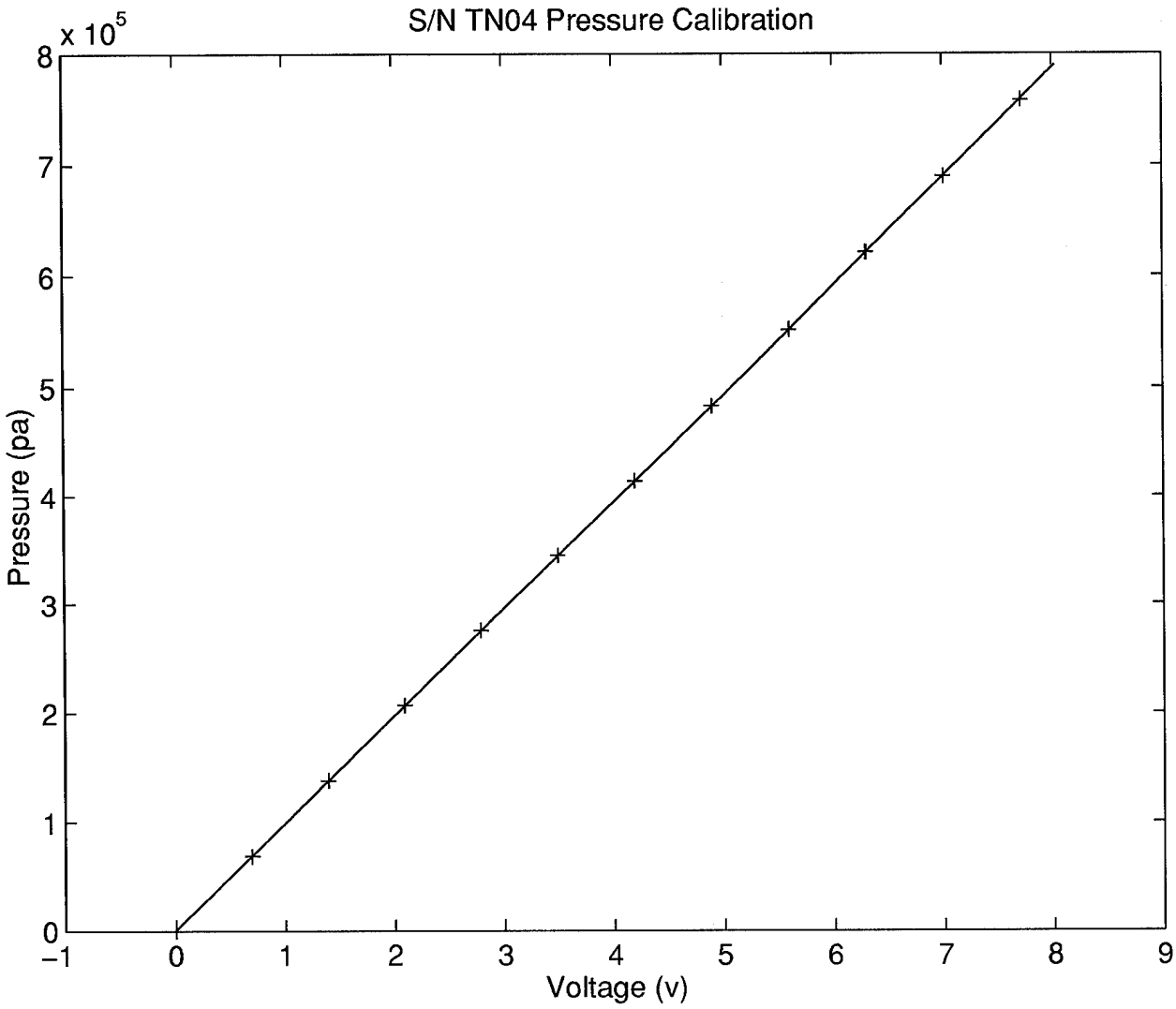

Figure A.9 Calibration For Pressure Transducer No.8

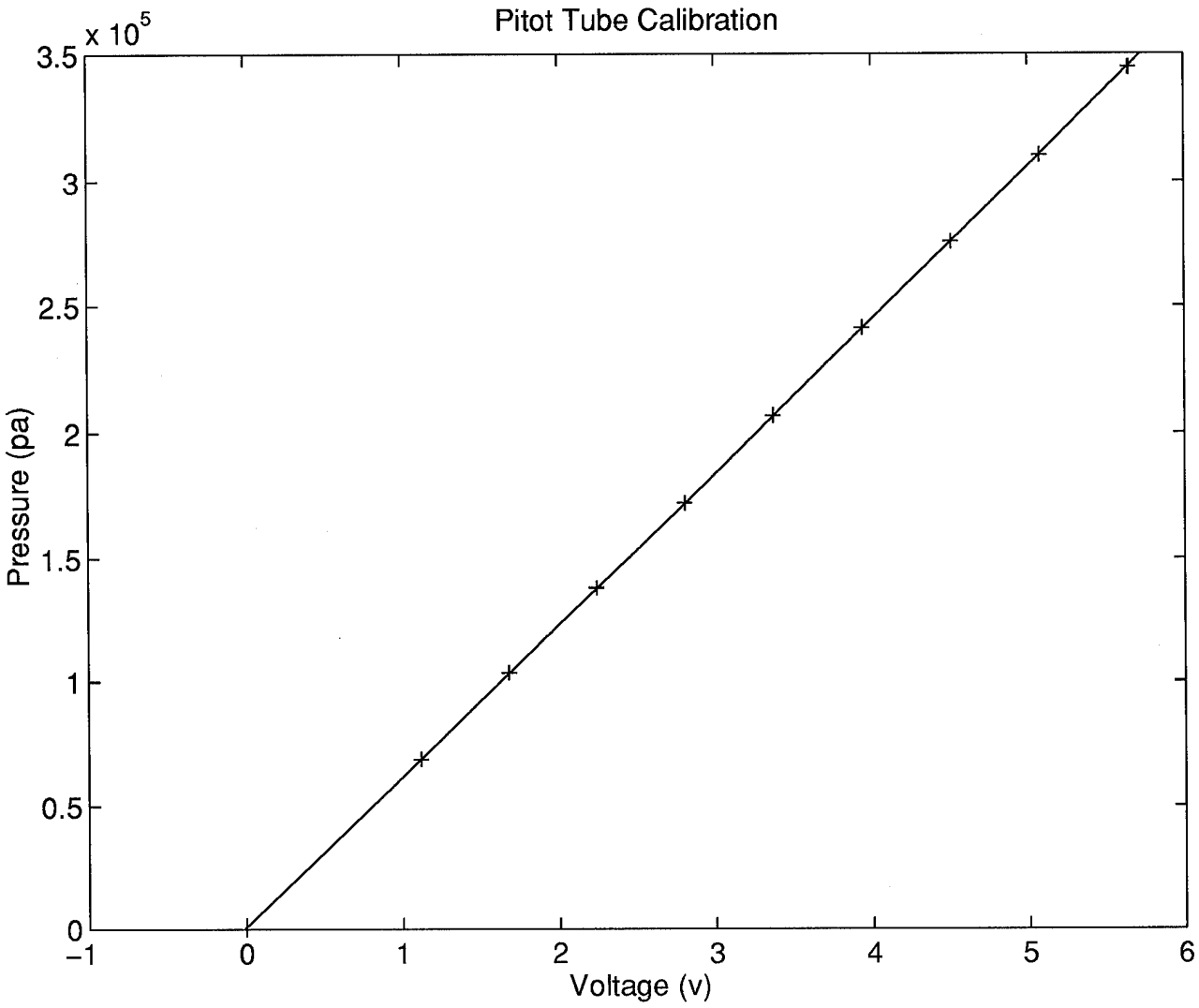

Figure A.10 Calibration For Pressure Transducer in Pitot Tube

Appendix B

The location of each heat flux gauge in the nozzle is shown in Fig $B.1$,

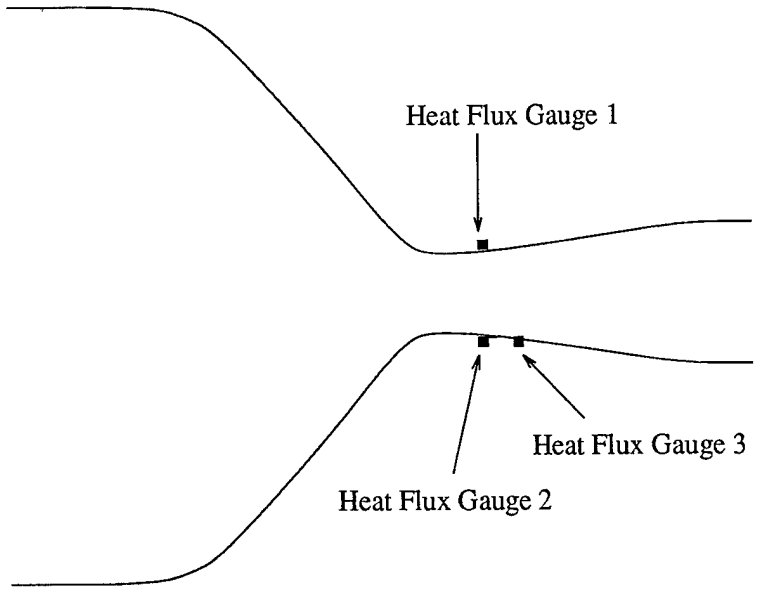

Figure B.1 Location of Heat Flux Gauges in the Nozzle

where the gauge 1,2 were 5.5 mm downstream of the nozzle throat, and the gauge 3 was 2.1 cm downstream of the nozzle throat.

The results of the calibration were shown in Fig $B.2$ through $B.4$, and the equations of the least square fit for these calibration were listed below.

Heat Flux Gauge Number	Serial Number	Linear Relation
No.1	S/N 58	$\Delta T = \frac{(v-0.003683)}{0.025809}$
No.2	S/N 48	$\Delta T = \frac{(v-0.001449)}{0.025134}$
No.3	S/N 530	$\Delta T = \frac{(v-0.0.002931)}{0.026848}$

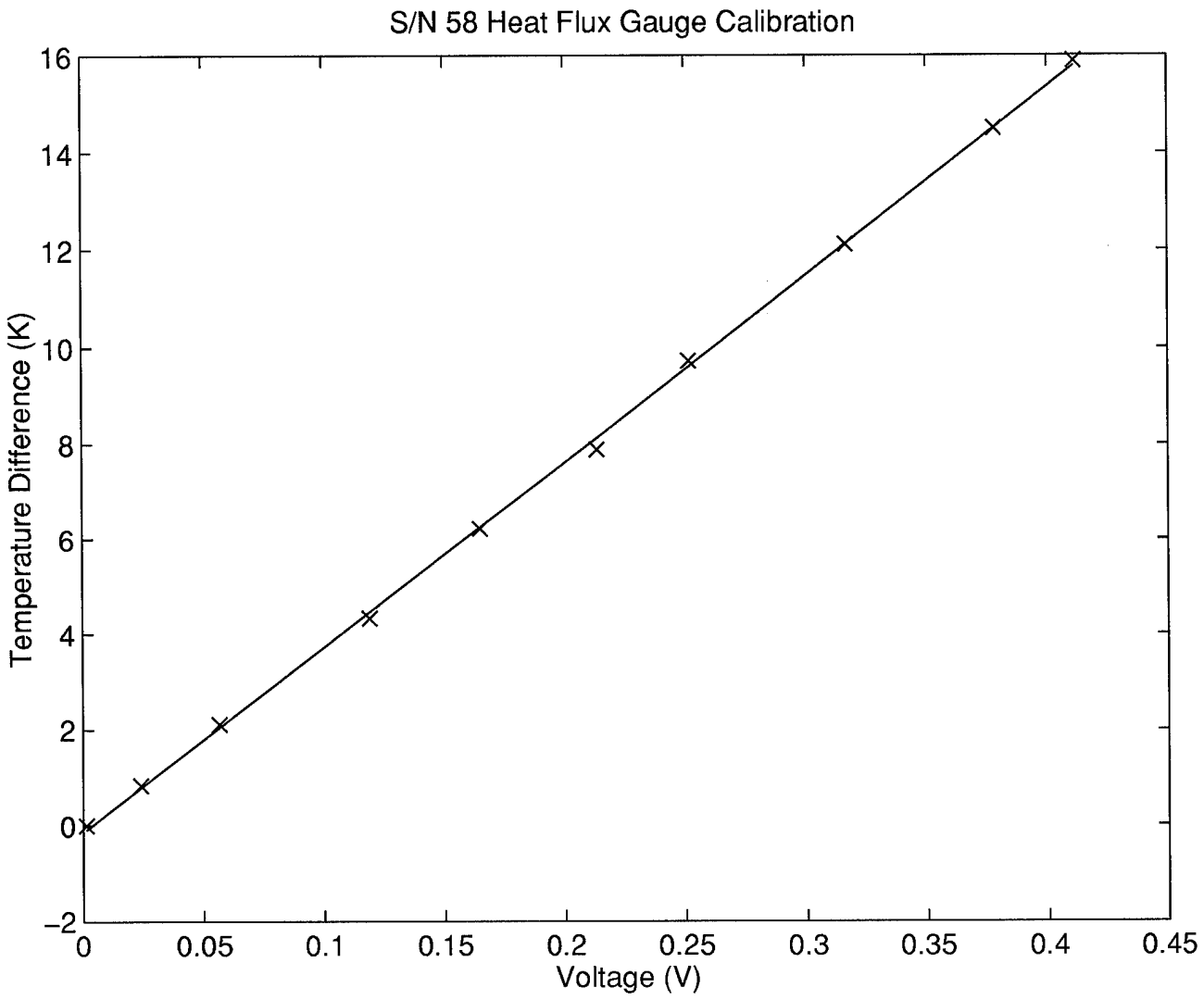

Figure B.2 Calibration For Heat Flux Gauge No.1

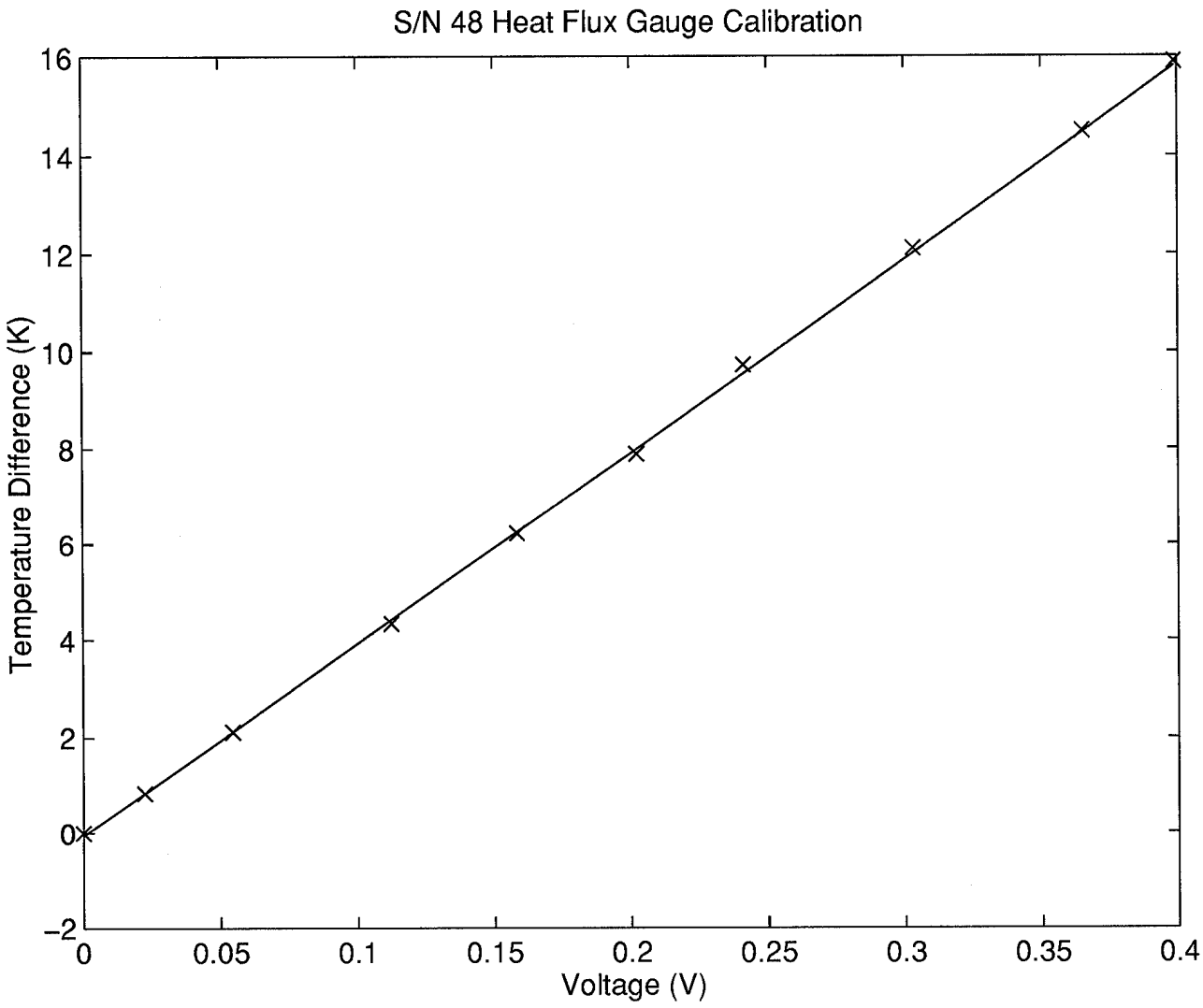

Figure B.3 Calibration For Heat Flux Gauge No.2

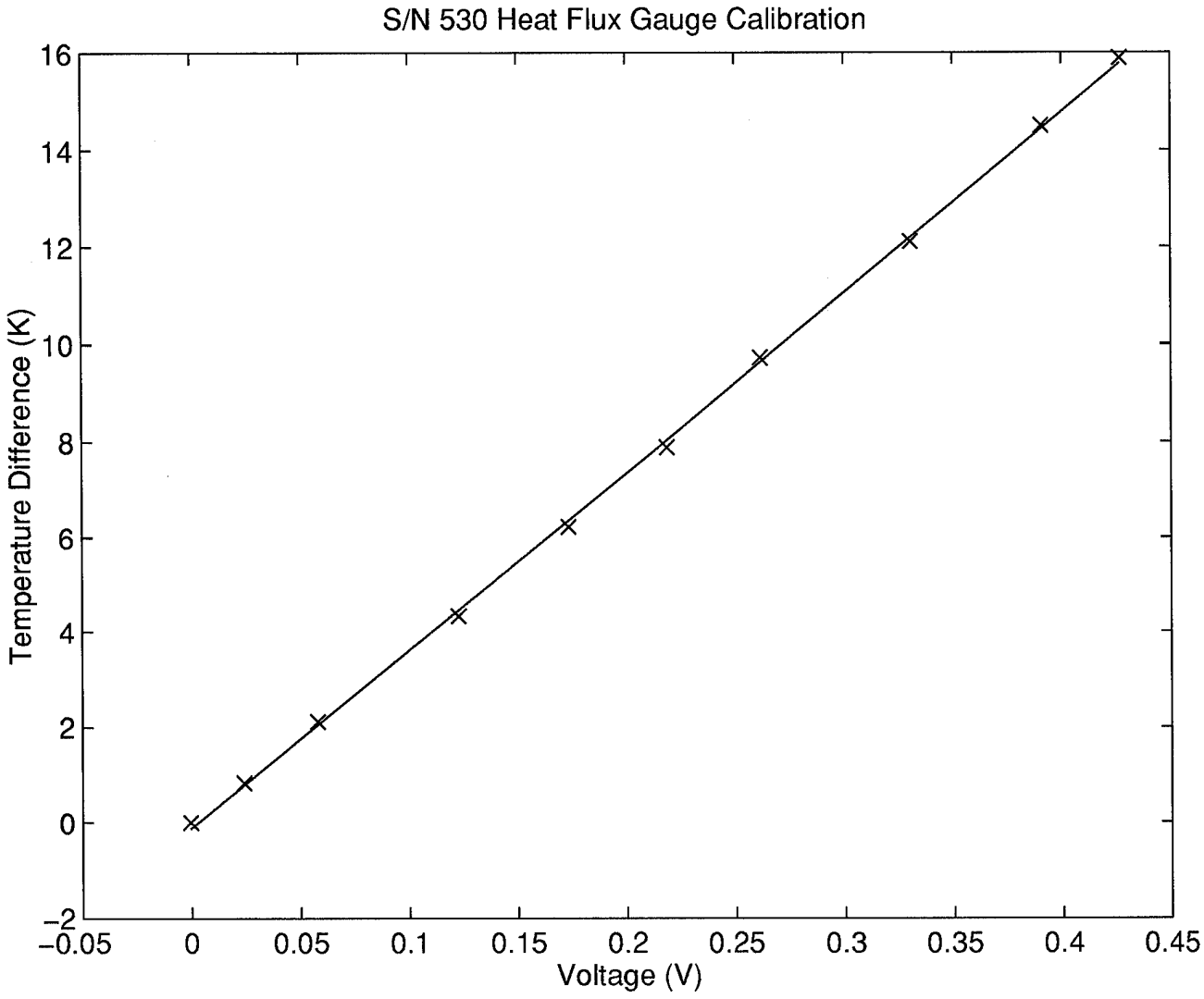

Figure B.4 Calibration For Heat Flux Gauge No.3

Bibliography

1. Anderson, John D. Jr. *Modern Compressible Flow* (2nd Edition). McGraw-Hill Publishing Company, 1990.
2. Azevedo, David. "Measured Thrust Losses Associated with Secondary Air Injection Through Nozzle Walls," *Journal of Propulsion and Power*, *9* (January 1993).
3. Bartz, D.Z. *Advance in Heat Transfer*, *2*. Academic Press NEW YORK, 1965.
4. Cook, W.J. and E.J. Feldman. "Reduction of Data From Thin-film Heat Transfer Gages," *AIAA*, *4* (March 1956).
5. Eckert, E.R.G. and John N.B. livingood. "Comparison of Effectiveness of Convection, Transpiration, and Film Cooling Methods with Air as Coolant," *NACA TN 3010* (October 1953).
6. Keener, David M. *Investigation of Boundary Layer and Performance Effects of Transpiration Cooling Through a Porous Plate in a Rocket Nozzle*. Master Thesis, School of Engineering, Air Force Institute of Technology, December 1994.
7. Lenertz, Joseph L. *Effects of Blowing Ratio on Heat Transfer to the Throat Region of a Porous-walled Nozzle*. Master Thesis, School of Engineering, Air Force Institute of Technology, December 1994.
8. Librizzi, Joseph and Robert J. Cresci. "Transpiration Cooling of a Turbulent Boundary Layer in an Axisymmetric Nozzle," *AIAA*, *2* (April 1964).
9. May, Lee R. and Wendel M. Burkhardt. "Transpiration Cooled Throat for Hydrocarbon Rocket Engine," *Journal of Spacecraft Propulsion and Power* (December 1991).
10. Mickley, H.S., R.C. Ross A.L. Squyer and W.E. Stewart. "Heat Mass and Momentum Transfer for Flow Over a Flat Plate with Blowing or Suction," *NACA TN 3208* (December 1967).
11. Mott, Metallurgical Corporation. "Technical Handbook for Precision Porous Metal Products," *Product Catalog No. 1000A. Farmington CT* (1986).
12. Schultz, D.L. and T.V. Jones. "Heat Transfer Measurements in Short Duration Hypersonic Facilities," *AGARD-AG-165* (February 1973).
13. Shapiro, Ascher H. *The Dynamic and Thermodynamics of Compressible Fluid Flow*, *2*. John Wiley and Sons Inc, 1953.
14. Sutton, George P. *Rocket Propulsion Element* (6th Edition). John Wiley and Son Inc., 1992.
15. Vidal, R.J. "Model Instrumentation Techniques for Heat Transfer and Force Measurement in a Hypersonic Shock Tunnel," *WADC TN 56-315* (1956).

16. Welsh, W.E. and A.B. Witt. "A Comparison of Analytical and Experimental Local Heat Fluxes in Liquid Propellant Rocket Thrust Chamber," *Jet Propulsion Lab. TR 32-43* (Feburary 1961).

17. Wright, J. K. *Shock Tube*. John Wiley and Sons Inc, 1961.

Vita

Maj. Chen Fu-Jung was born on 26 December 1958 in Taipei, Taiwan, R.O.C. He has four sisters. He graduated from Air Force Communication and Electronic School in 1980 and was assigned a job to maintain the Navigation Radar system at Ping-Tong AFB. He married in 1981. Two years later. he received an air communication system maintaince training for six months in Keesler AFB, U.S.A. In 1987, he attended Chung-Heing University. Upon graduation in 1990, he received his Bachelor of Science Degree in Mechanical Engineering. He entered the graduate School of Engineering, Air Force Institute of Technology in June 1993. Upon graduation, he will be ready to go back to his country.

Permanent address: 4F No.60 TeHsing W Rd
Taipei Taiwan R.O.C

REPORT DOCUMENTATION PAGE

Form Approved
OMB No. 0704-0188

1. AGENCY USE ONLY (Leave blank)	2. REPORT DATE	3. REPORT TYPE AND DATES COVERED
	June 1995	Master Thesis

4. TITLE AND SUBTITLE
Effects of Blowing Ratios on Heat Transfer to the Throat Region of a Porous-Walled Nozzle

5. FUNDING NUMBERS

6. AUTHOR(S)
Fu-Jung Chen

7. PERFORMING ORGANIZATION NAME(S) AND ADDRESS(ES)
Lt Col. Jerry Bowman
AFIT/ENY WPAFB OH

8. PERFORMING ORGANIZATION REPORT NUMBER
AFIT/GAE/ENY/95J-01

9. SPONSORING / MONITORING AGENCY NAME(S) AND ADDRESS(ES)
Mr. Terence Galati OLAC PL/RKCA, 4 Draco Dr.
Phillips Laboratory, Edwards AFB CA 93524-7190

10. SPONSORING / MONITORING AGENCY REPORT NUMBER

11. SUPPLEMENTARY NOTES

12a. DISTRIBUTION / AVAILABILITY STATEMENT
Approved for public release; distribution unlimited

12b. DISTRIBUTION CODE

13. ABSTRACT *(Maximum 200 words)*

The effects of transpiration cooling on heat transfer in the throat region of a porous-walled were investigated. The experiments were performed in the AFIT low pressure shock tube fitted with a Mach 2 nozzle. A blowing region was limited to the area 1.3 cm upstream to 1.2 cm downstream of the throat. Heat flux data were taken from both sides of the nozzle. One side was transpiration cooled by secondary air injection through a porous wall, while the other side was an impermeable surface. The results showed up to a 40% reduction in heat transfer coefficient at the blowing ratio of 0.0116. Also, the results of the exit Mach number and boundary layer thickness showed good improvement compared to a larger blowing region (from 1.3 cm upstream to 8.8 cm downstream of the throat).

14. SUBJECT TERMS
Porous Material, Heat Flux Gauge Calibration, Shock Tube, Heat Transfer, Transpiration Cooling, Blowing Ratio.

15. NUMBER OF PAGES
69

16. PRICE CODE

17. SECURITY CLASSIFICATION OF REPORT	18. SECURITY CLASSIFICATION OF THIS PAGE	19. SECURITY CLASSIFICATION OF ABSTRACT	20. LIMITATION OF ABSTRACT
Unclassified	Unclassified	Unclassified	UL

GENERAL INSTRUCTIONS FOR COMPLETING SF 298

The Report Documentation Page (RDP) is used in announcing and cataloging reports. It is important that this information be consistent with the rest of the report, particularly the cover and title page. Instructions for filling in each block of the form follow. It is important to ***stay within the lines*** to meet ***optical scanning requirements***.

Block 1. Agency Use Only *(Leave blank)*.

Block 2. Report Date. Full publication date including day, month, and year, if available (e.g. 1 Jan 88). Must cite at least the year.

Block 3. Type of Report and Dates Covered. State whether report is interim, final, etc. If applicable, enter inclusive report dates (e.g. 10 Jun 87 - 30 Jun 88).

Block 4. Title and Subtitle. A title is taken from the part of the report that provides the most meaningful and complete information. When a report is prepared in more than one volume, repeat the primary title, add volume number, and include subtitle for the specific volume. On classified documents enter the title classification in parentheses.

Block 5. Funding Numbers. To include contract and grant numbers; may include program element number(s), project number(s), task number(s), and work unit number(s). Use the following labels:

C	- Contract	**PR**	- Project
G	- Grant	**TA**	- Task
PE	- Program Element	**WU**	- Work Unit Accession No.

Block 6. Author(s). Name(s) of person(s) responsible for writing the report, performing the research, or credited with the content of the report. If editor or compiler, this should follow the name(s).

Block 7. Performing Organization Name(s) and Address(es). Self-explanatory.

Block 8. Performing Organization Report Number. Enter the unique alphanumeric report number(s) assigned by the organization performing the report.

Block 9. Sponsoring/Monitoring Agency Name(s) and Address(es). Self-explanatory.

Block 10. Sponsoring/Monitoring Agency Report Number. *(If known)*

Block 11. Supplementary Notes. Enter information not included elsewhere such as: Prepared in cooperation with...; Trans. of...; To be published in.... When a report is revised, include a statement whether the new report supersedes or supplements the older report.

Block 12a. Distribution/Availability Statement. Denotes public availability or limitations. Cite any availability to the public. Enter additional limitations or special markings in all capitals (e.g. NOFORN, REL, ITAR).

- **DOD** - See DoDD 5230.24, "Distribution Statements on Technical Documents."
- **DOE** - See authorities.
- **NASA** - See Handbook NHB 2200.2.
- **NTIS** - Leave blank.

Block 12b. Distribution Code.

- **DOD** - Leave blank.
- **DOE** - Enter DOE distribution categories from the Standard Distribution for Unclassified Scientific and Technical Reports.
- **NASA** - Leave blank.
- **NTIS** - Leave blank.

Block 13. Abstract. Include a brief *(Maximum 200 words)* factual summary of the most significant information contained in the report.

Block 14. Subject Terms. Keywords or phrases identifying major subjects in the report.

Block 15. Number of Pages. Enter the total number of pages.

Block 16. Price Code. Enter appropriate price code *(NTIS only)*.

Blocks 17. - 19. Security Classifications. Self-explanatory. Enter U.S. Security Classification in accordance with U.S. Security Regulations (i.e., UNCLASSIFIED). If form contains classified information, stamp classification on the top and bottom of the page.

Block 20. Limitation of Abstract. This block must be completed to assign a limitation to the abstract. Enter either UL (unlimited) or SAR (same as report). An entry in this block is necessary if the abstract is to be limited. If blank, the abstract is assumed to be unlimited.

★U.S.GPO:1993-0-336-043